

Investigation of rarely measured VOCs emitted from wheat residue fires in the summer time air of N.W. Indo-Gangetic Plain

Bharti Sohpaal

MS12102

*A dissertation submitted for the partial fulfilment of
BS-MS dual degree in Science*



**Indian Institute of Science Education and Research Mohali
April 2017**

Certificate of Examination

This is to certify that the dissertation entitled “**Investigation of rarely measured VOCs emitted from wheat residue fires in the summer time air of N.W. Indo-Gangetic**” submitted by **Ms. Bharti Sohpaal** (MS12102) for the partial fulfilment of BS-MS dual degree programme of the Institute, has been examined by the thesis committee duly appointed by the Institute. The committee finds the work done by the candidate satisfactory and recommends that the report be accepted.

Dr. V. Sinha
(Supervisor)

Dr. B. Sinha

Dr. P. Balanarayan

Dated: April 21, 2017

Declaration

The work presented in this dissertation has been carried out by me under the guidance of Dr. V. Sinha at the Indian Institute of Science Education and Research Mohali.

This work has not been submitted in part or in full for a degree, a diploma, or a fellowship to any other university or institute. Whenever contributions of others are involved, every effort is made to indicate this clearly, with due acknowledgement of collaborative research and discussions. This thesis is a bonafide record of original work done by me and all sources listed within have been detailed in the bibliography.

Bharti Sohpaal
(Candidate)

Dated: April 21, 2017

In my capacity as the supervisor of the candidate's project work certify that the above statements by the candidate are true to the best of my knowledge.

Dr. V. Sinha
(Supervisor)

Acknowledgment

I would like to express my gratitude to Dr. Vinayak Sinha, my project supervisor for his kind supervision and guidance in completing my dissertation. I would also like to thank Dr. N. Sathyamurthy, Director, IISER Mohali and Prof. P. Guptasarma, Dean R&D, IISER Mohali for providing a conducive environment which was very helpful for completing the thesis in time. I am thankful to Dr. Baerbel Sinha and Dr. P. Balanarayan for providing their valuable inputs.

I also acknowledge my lab mates B. Praphulla Chandra, Harshita Pawar, Ashish Kumar, Haseeb Hakkim, Abhishek Mishra, Vinod Kumar, Saryu Garg, Gaurav Sharma, Savita Dutta, Pallavi Janagra, Ebin George, Nimya Sunil and Mohammad Shabin for their assistance.

List of Figures

1.2.1: Degradation schematic of 1,2,3-trimethylbenzene with hydroxyl radical.....	24
1.2.2: Mechanism of the ring-cleavage reactions in the photooxidation of o-xylene.....	26
1.2.3: Mechanism of reaction of methyl ethyl ketone with hydroxyl radical in water	27
1.2.4: Time-concentration profiles for o-xylene, biacetyl, and PAN	29
1.2.5: Photolysis of 2,3-butanedione and formation of peroxyacetyl nitrate.....	30
2.1.1: Location of Mohali, in the NW-IGP and map of the land use in a 100 km×200	33
2.1.2: Total number of fire counts detected in 2013 by MODIS satellite over N.W.IGP.	35
2.1.3: Daily fire counts detected by MODIS over N.W.IGP	36
2.2.1: Wind rose plot for the measurement site for pre-harvest and post-harvest period.....	37
2.2.2: Diel profile of RH, ambient temperature, wind speed, and solar radiation	37
2.3.1: Schematic of the proton transfer reaction mass spectrometer	39
2.4.1: Sensitivity and linearity of selected VOCs.....	42
2.4.2: Calibration factors for PTR-MS vs mass of the calibrated species	43
3.1.1: Chemical structure of VOCs identified in this work	48
3.2.1: Time series for the ambient concentrations of acetonitrile and 2,3-butanedione.	49
3.2.2: Time series of mixing ratio of 2,3-butanedione (dark green) and solar radiation.	50
3.2.3: Correlation plot of 2,3-butanedione with C-9 aromatics and C-8 aromatics.....	51
3.3.1: Diel profile for mixing ratios of frequently quantified VOCs and rarely measured VOCs.....	54
3.3.2: Correlation plot propene with acetic acid.....	56

3.5.1: Correlation plots of all the reported VOCs with acetonitrile.....	61
3.5.2: Diel box and whisker plot of CO and correlation plot of acetonitrile and carbon monoxide.....	63
3.5.3: Major VOCs that were emitted from wheat residue fires.....	64
3.6.1: Contribution of different class of compounds to total reactive carbon.	66
3.6.2: Contribution of individual VOCs to total O ₃ formation potential	68
3.7.1: SOA formation potential of isoprene, benzene, toluene, xylenes, trimethylbenzenes, naphthalene and styrene	71
3.8.1: Scatter plots of all the VOCs versus benzene/C-9 aromatics..	74
3.8.2: Diurnal profile of anthropogenic contribution and observed total concentration of VOCs	77
3.8.3: Anthropogenic fraction of all the VOCs during the pre-harvest and post-harvest period.....	78

List of Tables

1.2.1: Percentage yield of 2,3-butanedione in the photooxidation of TMB.	25
1.2.2: Percentage yield of 2,3-butanedione in the photooxidation of o-xylene	26
1.2.3: Emission factors of acetonitrile and 2,3-butanedione	31
2.2.1: Average ambient temperature, RH, wind speed and most frequent wind direction.	38
2.4.1: Compound-specific VOC m/z assignments, nominal protonated m/z ratios, sensitivity, limit of detection and uncertainty.....	44
3.4.1: Results of Mann-Whitney U test for the daytime data.	57
3.4.2: Results of Mann-Whitney U test for the nighttime data.....	58
3.5.1: Ratio of average daytime concentration to average nighttime concentration of VOCs during pre-harvest and post-harvest period.....	62
3.7.1: SOA yields of VOCs	70

Notation (Abbreviations)

- | | |
|---------------|---|
| 1. VOC | Volatile Organic Compounds |
| 2. NW-IGP | North West - Indo Gangetic Plain |
| 3. NMOC | Non-methane organic compounds |
| 4. BB | Biomass burning |
| 5. PTR-MS | Proton-transfer reaction mass spectrometer |
| 6. NIOSH | National Institute for Occupational Safety and Health |
| 7. GC-PTR-MS | Gas chromatography coupled to PTR-MS |
| 8. PTR-TOF-MS | PTR - “Time-of-Flight”- mass spectrometer |
| 9. P.A. | Proton affinity |

Content

List of Figures.....	9
List of Tables	13
Notation (Abbreviations).....	15
Content.....	17
Abstract.....	19
1 Introduction	21
1.1 Volatile Organic Compounds from Biomass Burning	21
1.2 2,3-Butanedione: Sources, Sinks and Health Impacts.....	22
1.2.1 Photo-oxidation of 1,2,3- and 1,2,4-Trimethylbenzene	23
1.2.2 Photooxidation of o-Xylene.....	25
1.2.3 Photo-oxidation of methyl ethyl ketone in aqueous phase	26
1.2.4 Atmospheric Fate of 2,3-Butanedione	28
1.2.5 Studies which have quantified 2,3-butanedione from biomass burning	30
2 Material and methods	33
2.1 Site description and basis for selection of time span of pre-harvest and post-harvest season	33
2.2 Prevalent meteorology.....	36
2.3 Volatile organic compound measurements using a proton transfer reaction mass spectrometer	39
2.4 Data quality assurance.....	40
2.4.1 Calibration procedure.....	40
2.4.2 Data Quality Assurance to exclude local pollution events	46
3 Results and discussion	47
3.1 Identification of rarely measured VOCs in the summer time air of NW-IGP	47
3.2 Chemistry of 2,3-butanedione	48
3.3 Diel concentration profiles of VOCs during pre-harvest and post-harvest periods ..	51
3.4 Statistical tests for assessing significance of variation in the ambient concentration of VOCs during pre-harvest and post-harvest periods	56

3.5	VOC/acetonitrile emission ratios during pre and post-harvest periods.....	59
3.6	Total reactive carbon and ozone production potential of VOCs during pre and post-harvest periods.....	65
3.7	SOA formation potential of VOCs.....	69
3.8	Constraining the anthropogenic contribution to VOC concentrations: Evaluation of an approach extant in literature.....	72
4	Summary and conclusion.....	79
5	Bibliography.....	81

Abstract

Biomass burning is a significant source of reactive and toxic ambient volatile organic compounds. Every year, extensive wheat crop residue burning ($> 5500 \text{ km}^2$) occurs during the months of April-May in the North West Indo-Gangetic Plain (NW- IGP). The gases and particles emitted from such fires impact atmospheric chemical processes, the biosphere and human health (e.g. benzene, a human carcinogen, is emitted from such fires). Till date, there has been no study in NW-IGP quantifying the contribution of wheat residue burning on the ambient mixing ratios of volatile organic compounds. Here, using a high sensitivity proton-transfer reaction mass spectrometry we have quantified 27 different organic compounds ($n \geq 47504$ in pre-harvest and $n \geq 17260$ in post-harvest for each species), which were likely emitted (at a confidence interval of 99.99 %) from the regional post-harvest wheat residue fires. Out of 27 VOCs, 14 VOCs were reported for the first time over N.W. IGP and those newly reported VOCs are propyne, propene, formamide, formic acid, acrolein, methylketene, acetamide, acetic acid, nitromethane, hydroxyacetone, 2,3-butanedione, 2-furaldehyde, styrene and naphthalene. The measurements were performed at the IISER Mohali Atmospheric Chemistry Facility, a sub-urban site in the NW-IGP from February 2013 – May 2013, spanning both the pre and post wheat harvest periods. The post-harvest period was characterized by significantly high concentrations of acetonitrile (chemical marker for biomass burning), carcinogenic benzenoids, methanol, acetaldehyde, nitromethane, hydroxyacetone and other VOCs. The average mixing ratios (average $\pm 1\sigma$ ambient variability) of acetonitrile ($1.35 \pm 1.30 \text{ ppb}$) and 2,3-butanedione ($2.35 \pm 1.08 \text{ ppb}$) in post-harvest period were higher by a factor of 1.8 relative to pre-harvest period. Different VOC/acetonitrile emission ratios and high absolute concentrations during post-harvest period in comparison to pre-harvest period implies altered source signatures in post-harvest period with strong contribution from biomass fires. A new compound, i.e., 2,3-butanedione (most

plausible identity for $m/z = 87$) was also detected and reported for the first time in ambient Indian air. It has both primary (wheat residue fires) and secondary sources (oxidation of trimethylbenzenes) and its major fate is photolysis resulting in formation of peroxyacetyl nitrate, an ingredient of urban smog. Major VOC emissions due to the post-harvest fires were constrained and ranked as follows: methanol (5.28 Gg) > acetone (1.53 Gg) > propene (0.75 Gg) > benzene (0.58 Gg). The total average reactive carbon due to all 27 VOCs during pre-harvest and post-harvest period was 259.7 ppbC and 496.6 ppbC, respectively. The total O_3 production potential due to 22 VOCs during post-harvest period was higher by a factor of 1.7 relative to pre-harvest period for both morning (06:00 to 12:00 LT) and afternoon (12:00 to 18:00 LT) times. These results help explain the 19 ppb enhancement in surface ozone concentrations during post-harvest wheat residue fires as reported by Kumar et al. (2016). The four major contributors were isoprene (26–31 %), acetaldehyde (24 %), acrolein (13-14 %) and 2-furaldehyde (7-9 %), which collectively accounted for more than 72 % of the total O_3 formation potential. The order of SOA formation potential for VOCs in pre-harvest period was benzene > toluene > xylenes > naphthalene > trimethylbenzenes > isoprene > styrene, whereas the order in post-harvest period was benzene > toluene > naphthalene > xylenes > trimethylbenzenes > isoprene > styrene. This study provides the first detailed experimental evidence of the large scale perturbation to ambient VOC chemical composition and secondary pollutant formation in the N.W. IGP which strongly impairs the regional air quality.

Chapter 1

1 Introduction

1.1 Volatile Organic Compounds from Biomass Burning

Volatile organic compounds (VOCs) are the organic compounds that have a vapor pressure greater than 0.01kPa at 298K and low boiling points (323K to 533K) at 1.013 bar pressure. Globally, every year ~ 1300 TgC (Goldstein and Galbally, 2007) of chemically diverse VOCs are emitted into the atmosphere. Biomass burning (BB) releases large suite of trace gases and carbonaceous particles in the atmosphere, such as CO, CO₂, PM_{2.5}, and black carbon, which can cause lung and respiratory diseases. BB emits 406 Tg yr⁻¹ of non-methane organic compounds (NMOC) and thus it is the second largest global source of NMOC (Akagi et al., 2011). The burning of crop residue is regarded as the fourth largest type of BB (Akagi et al., 2011, Andreae and Merlet, 2001). Globally, the estimated crop residue biomass consumption for burning of fields is 489 Tg per year (Akagi et al., 2011). Typically 116-289 Tg of crop residue is burnt in India annually (Venkataraman et al., 2006). Every year, extensive wheat crop residue burning occurs during the months of April-May in the NW Indo-Gangetic Plain (N.W.IGP). The use of combine harvester technology leaves large amount of wheat straw on the field. To get rid of the straw and prepare the field for next sowing season, the farmers set it on fire as it is the easiest, cheapest and quickest method of clearing the field. More than 5500 km² of land area is typically burnt in Punjab during May. It can contribute 113 Gg of

CO, 8.6 Gg of NO_x, 13 Gg of PM₁₀ and 12 Gg of PM_{2.5} (Badarinath et al., 2006). Hence, wheat residue burning is a considerable source of greenhouse gases in the atmosphere. About 284 Tg of crop residue is burnt annually in India, of which 40% is from wheat residue (Sahai et al., 2007). The pollutants from crop residue burning are substantial in Indo-Gangetic Plain as about 12 * 10⁶ ha of land is practiced for rice-wheat crop rotation (Badarinath et al., 2006). The estimated amount of wheat residue yield generated in Punjab is 3.2 – 5.6 tonnes per hectare (Badarinath et al., 2006). Typically 116-289 Tg of crop residue is burnt annually in India (Venkataraman et al., 2006). Apart from the emissions of toxic VOCs, crop residue burning also results in decline in soil biota and other soil properties such as loss of nutrients and decreased soil fertility (Kushwaha and Singh, 2005). The pollutants emitted from agricultural residue fires have serious implications on atmospheric chemical processes, biosphere and human health (e.g. benzene which is a class A carcinogen is emitted from such fires). These organic compounds upon reaction with oxides of nitrogen (NO_x) in the presence of sunlight fuel the formation of surface ozone, which is a criteria air pollutant and an important greenhouse gas. Summertime ozone in the N.W. IGP has direct harmful impact on human health and other living organisms. It is the main source of tropospheric OH radicals which determines the oxidation capacity of the atmosphere. Physical and chemical processing of VOCs converts them to less volatile products and also form secondary organic aerosols (SOA). These secondary organic aerosols tend to increase the mass concentration of particulate matter in the atmosphere and hence alter its radiative properties.

1.2 2,3-Butanedione: Sources, Sinks and Health Impacts

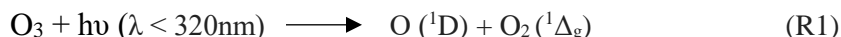
2,3-Butanedione, also known as biacetyl or diacetyl, is a vicinal diketone with the chemical formula (CH₃CO)₂. The chemical structure of 2,3-butanedione is shown in *Figure 3.1.1*. 2,3-Butanedione exposures have a close affinity with lower pulmonary function. It is known to

cause constrictive bronchiolitis obliterations (chronic scarring and severe narrowing of the bronchiole airways) and decrease in lung function. The National Institute for Occupational Safety and Health (NIOSH), USA recommends exposure limit below a concentration of 5 ppb as a time-weighted average for up to 8 hours/day during a 40-hour work week. It also recommends a short-term exposure limit of 25 ppb for a 15-minute time period (McKernan et al., 2016). The major sources of 2,3-butanedione in the atmosphere are:

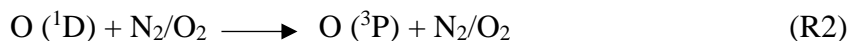
- (1) **Primary Source:** The primary emissions of 2,3-butanedione occurs from biomass fires.
- (2) **Secondary Source:** It is formed photochemically through hydroxyl radical initiated reactions of 1,2,3-trimethylbenzene, 1,2,4-trimethylbenzene, ortho-xylene and methyl ethyl ketone in the aqueous phase. Currently, the global budgets of 2,3-butanedione have not been estimated to the best of our knowledge.

1.2.1 Photo-oxidation of 1,2,3- and 1,2,4-Trimethylbenzene

Once emitted into the atmosphere, reactivity of xylenes and trimethylbenzenes with hydroxyl radical controls their removal rates. Photolysis of ozone in the presence of water vapor is the main source of hydroxyl radicals in the troposphere.



The fate of ~90% O (¹D) atoms is collisional quenching via



Up to 10% of O (¹D) reacts with water vapor to give two OH radicals



The photooxidation of trimethylbenzene can either proceed via H-abstraction by OH radicals or 1,2 addition of OH to the aromatic ring. The H-abstraction from alkyl substituent yield a carbonyl compound after a series of chemical reactions involving NO_x and HO_x. The reaction pathway for the photo-oxidation of 1,2,3-trimethylbenzene in atmosphere is

illustrated in *Figure 1.2.1*. The dominant reaction pathway is the electrophilic addition of hydroxyl radical primarily at the ortho position of each side chain followed by addition of O₂ to the OH-aromatics adduct. It further undergoes a cyclization reaction to form a bicyclo- (-O-O-bridge) compound. After the addition of O₂ to this bicyclo compound and subsequent abstraction of an O atom by NO to form NO₂, an alkoxy-type radical is generated. This alkoxy-type radical undergoes ring cleavage and yields an unsaturated γ-dicarbonyl and a 1-hydroxy-2-oxoalkyl radical (R-C(OH)-CR'=O). This radical generates α-dicarbonyl after the hydrogen abstraction by O₂ (Bandow and Washida, 1985b). The reaction which involves the oxidation of NO to NO₂, also involves the formation of tropospheric ozone as the photolysis of NO₂ gives an O(³P) atom that combines with O₂ and hence forms O₃.

The rate constant of 1,2,3-trimethylbenzene and 1,2,4-trimethylbenzene with OH is $3.27 \times 10^{-11} \text{ cm}^3 \text{ molecule}^{-1} \text{ s}^{-1}$ and $3.25 \times 10^{-11} \text{ cm}^3 \text{ molecule}^{-1} \text{ s}^{-1}$, respectively (Atkinson and Arey, 2003). The photo-oxidation of 1,2,4-trimethylbenzene has a similar reaction mechanism as that of 1,2,3-trimethylbenzene. Glyoxal and methylglyoxal are other products formed in the process of photo-oxidation. The yield of 2,3-butanedione was determined from the regression slopes of correlation plots between the amount of product formed and trimethylbenzene consumed. *Table 1.2.1* shows the percentage yield of 2,3-butanedione of trimethylbenzene consumed as reported by other chamber studies.

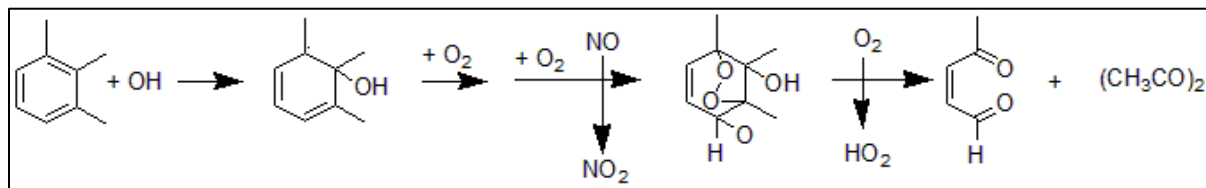


Figure 1.2.1: Degradation schematic of 1,2,3-trimethylbenzene with hydroxyl radical (Bandow and Washida, 1985b).

% Yield	2,3-butanedione	
1,2,3-trimethylbenzene	(Bandow and Washida, 1985b)	45 ± 2 %
	(Tuazon et al., 1986)	31.6 ± 3.6 %
1,2,4-trimethylbenzene	(Bandow and Washida, 1985b)	11 ± 1 %
	(Tuazon et al., 1986)	4.8 ± 0.9 %

Table 1.2.1: Percentage yield of 2,3-butanedione (mole/mole) in the photooxidation of trimethylbenzenes. The error is indicated as one standard deviation.

1.2.2 Photooxidation of o-Xylene

The reaction pathway for the photo-oxidation of o-xylene in atmosphere is illustrated in *Figure 1.2.2*. The addition of hydroxyl radical to xylene primarily occurs at the ortho position. The rate constant of o-xylene with OH is $1.36 \times 10^{-11} \text{ cm}^3 \text{ molecule}^{-1} \text{ s}^{-1}$ (Atkinson and Arey, 2003). The subsequent reactions are similar to the photooxidation of 1,2,3-trimethylbenzene which is explained above. 2,3-Butanedione is formed in the process of oxidation via a bridged bicyclic peroxy radical and is a co-product of butenedial (Bandow and Washida, 1985a). *Table 1.2.2* shows the percentage yield of 2,3-butanedione of o-xylene consumed as reported in various chamber studies. The large range of the yields reported by different studies could be due to the difficulty in handling α -dicarbonyls.

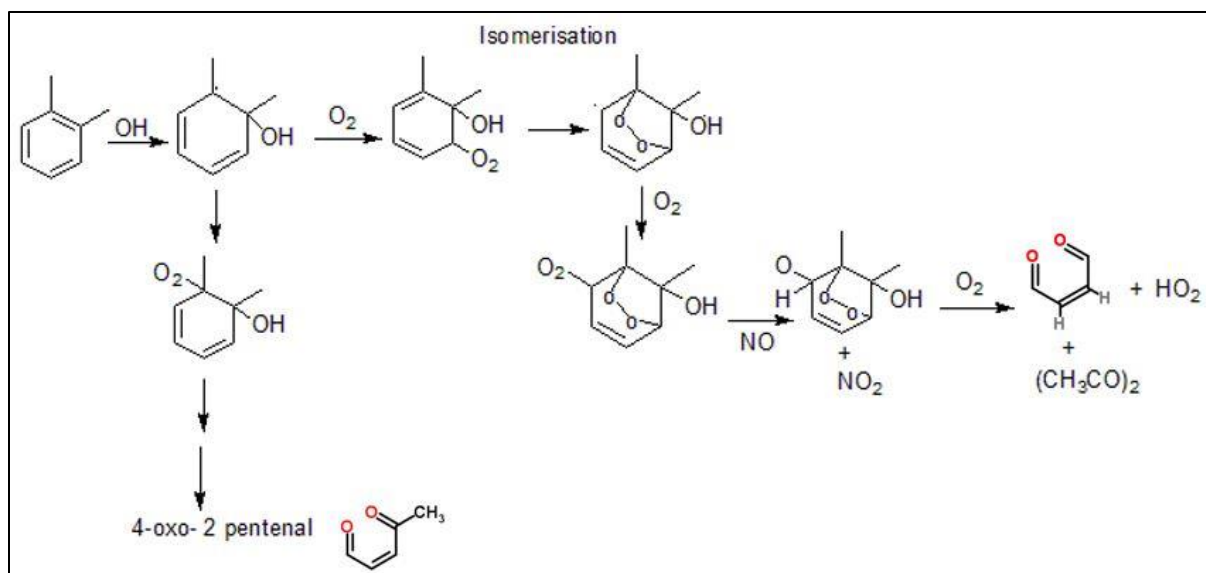


Figure 1.2.2: Mechanism of the ring-cleavage reactions in the photooxidation of o-xylene (Bandow and Washida, 1985a)

Yields (%)	(Nojima et al., 1974)	(Takagi et al., 1980)	(Darnall et al., 1979)	(Shepson et al., 1984)	(Atkinson et al., 1983)	(Bandow and Washida, 1985a)
2,3-Butanedione	1.2	26 ± 10	18 ± 4	8.5	13.7 ± 1.6	10 ± 2

Table 1.2.2: Percentage yield of 2,3-butanedione (mole/mole) in the photooxidation of o-xylene

1.2.3 Photo-oxidation of methyl ethyl ketone in aqueous phase

The reaction pathway for the photo-oxidation of methyl ethyl ketone (MEK) in aqueous phase is illustrated in *Figure 1.2.3*. This reaction occurs at a pH of 1. The H-abstraction by hydroxyl radical can take place at 3 different sites in the structure of methyl ethyl ketone. Note that the attack at carbon 3 leads to a secondary alkyl radical whereas attack at the terminal carbon yields a primary alkyl radical. The branching ratio for primary/secondary H-atom abstraction at the methyl ethyl ketone skeleton is 60/40. Only the secondary alkyl

radical chain leads to the formation of 2,3-butanedione. This radical rapidly reacts with oxygen to form alkylperoxy radicals which then recombine to form a tetroxide. The reaction can then proceed in three different pathways, i.e., (i) the formation of two carbonyl compounds and H_2O_2 , (ii) the formation of carbonyl compound and an alcohol, and (iii) decomposition into an alkoxy radical. Only the (ii) pathway leads to the formation of 2,3-butanedione and the other product formed in the reaction is 3-hydroxy-2-butanone. The major oxidation product i.e. 2,3-butanedione reaches a maximum yield of $29.5 \pm 6.0\%$ after 60 minutes of reaction. Photolysis of MEK is also an additional source of 2,3-butanedione with a molar yield of 2.2% (Rodigast et al., 2016).

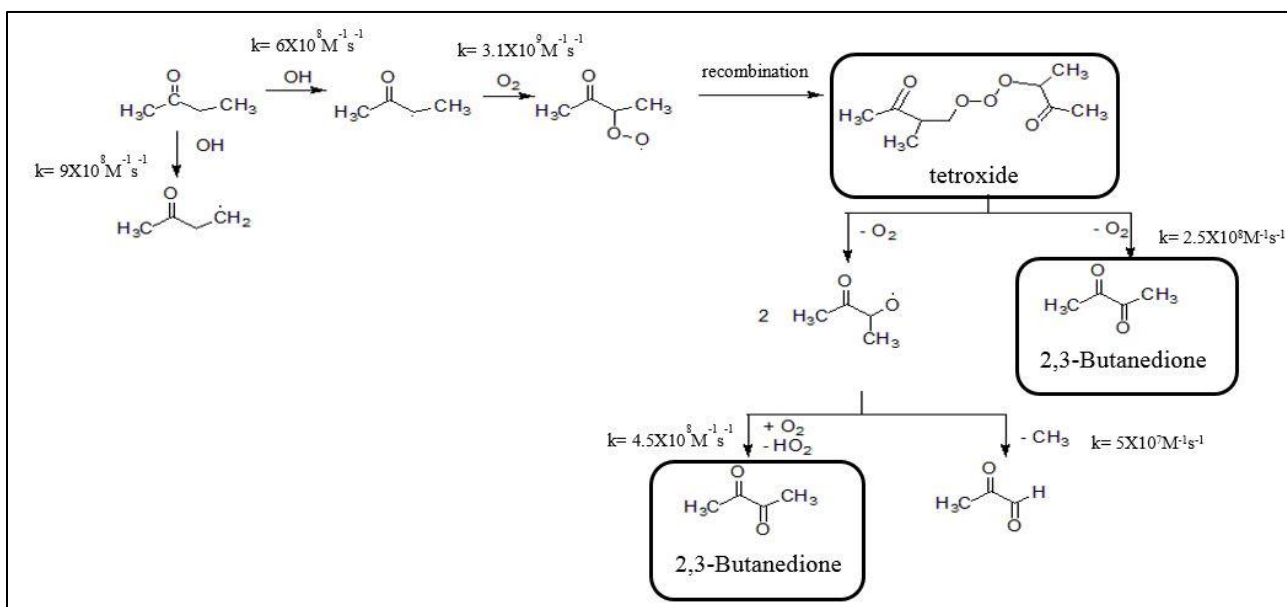


Figure 1.2.3: Mechanism of reaction of methyl ethyl ketone with hydroxyl radical in water to form 2,3-butanedione (Rodigast et al., 2016)

1.2.4 Atmospheric Fate of 2,3-Butanedione

1.2.4.1 Reaction with hydroxyl radical

The lifetime of a compound is defined as the time taken for its concentrations to reduce 1/e of its initial value. The rate coefficient for the reaction of OH and 2,3-butanedione at 298 K (pressure = 3333 - 6666 Pa) is $2.3 (\pm 0.2) \times 10^{-13} \text{ cm}^3 \text{ molecule}^{-1} \text{ s}^{-1}$ (Dagaut et al., 1988, Darnall et al., 1979). The lifetime of 2,3-butanedione with respect to reaction with OH can be calculated as follows:

$T = \text{concentration of compound} / \text{removal rate}$

$$T = \frac{[2,3\text{-butanedione}]}{k_{\text{OH}+2,3\text{-butanedione}} \times [\text{OH}] \times [2,3\text{-butanedione}]} \quad (1)$$

$$[\text{OH}] = 10^6 - 10^7 \text{ molecule cm}^{-3}$$

$$T \sim 5 \text{ to } 50 \text{ days}$$

The atmospheric lifetime of 2,3-butanedione due to reaction with OH radicals at a zenith angle of 0° is reported to be $T \geq 900 \text{ h}$ i.e. $\geq 38 \text{ days}$ (Plum et al., 1983), which lies in the range of the lifetime calculated above.

1.2.4.2 Photolysis

Photolysis is the dominant removal process of 2,3-butanedione from troposphere. The photolysis rate is $5 (\pm 0.3) \times 10^{-5} \text{ s}^{-1}$ (Plum et al., 1983). The atmospheric lifetime with respect to photolysis is 1 h (Plum et al., 1983). *Figure 1.2.4* shows the time concentration profile of o-xylene, 2,3-butanedione (also called biacetyl) and peroxyacetylnitrate (PAN). It indicates that initially 2,3-butanedione (biacetyl) is formed from the reaction of o-xylene with hydroxyl radicals and the product of this reaction i.e., biacetyl reaches a maximum concentration within 2 hours of irradiation.

Photooxidation of 2,3-butanedione forms peroxyacetyl nitrate (Darnall et al., 1979). Photolysis of 2,3-butanedione generates two CH_3CO radicals, which then reacts with O_2 and NO_2 to yield peroxyacetyl nitrate (PAN). This reaction is illustrated in *Figure 1.2.5*. PAN is a long-lived reservoir for nitrogen oxides (NO_x) and a lachrymator. It can alter the ozone production regime at the receptor site. It inhibits photosynthesis (Koukol et al., 1967) and is also an ingredient of photochemical smog. One would expect 2 moles of PAN being formed from 1 mole of 2,3-butanedione consumed, but in real atmosphere only 0.7 mole of PAN is formed per 2,3-butanedione photodissociated. It is because NO and NO_2 both compete for CH_3CO_3 radicals (Darnall et al., 1979).

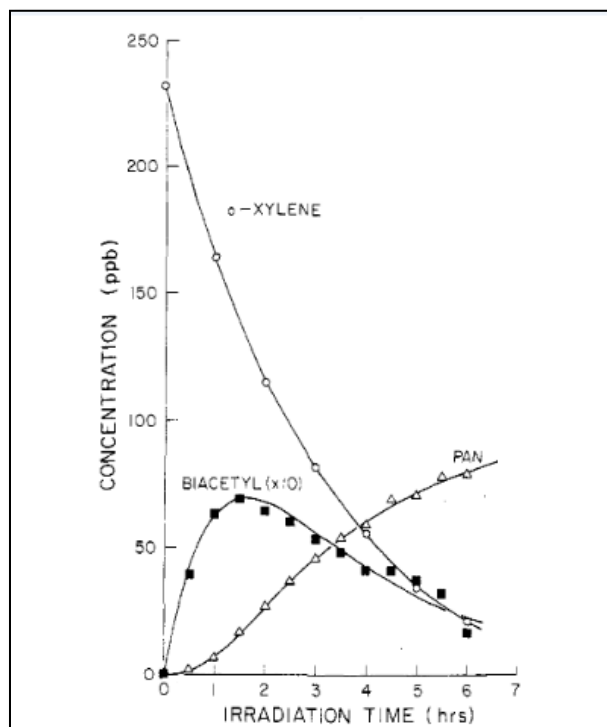


Figure 1.2.4: Time-concentration profiles for o-xylene, biacetyl, and PAN for a 6-h irradiation of NO , (0.48 ppm)/o-xylene (0.23 ppm)/air mixture at 303 K and atmospheric pressure (Darnall et al., 1979)

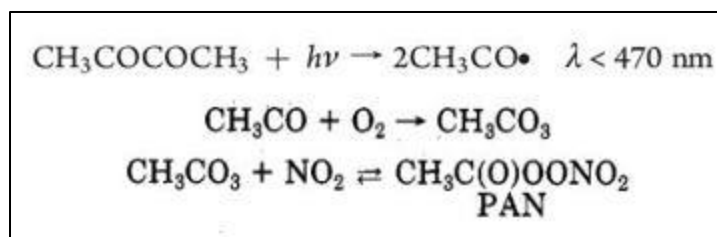


Figure 1.2.5: Photolysis of 2,3-butanedione and formation of peroxyacetyl nitrate (Darnall et al., 1979)

1.2.5 Studies which have quantified 2,3-butanedione from biomass burning

Due to analytical challenges associated with its quantification, very few studies have previously reported 2,3-butanedione and most were laboratory studies. Karl et al. (2007) quantified the emissions of 2,3-butanedione from tropical forest fuels burnt in the laboratory using gas chromatography coupled to proton-transfer reaction mass spectrometer (GC-PTR-MS). It was attributed as the major species (80%) at mass channel $m/z = 87$, with minor contributions from 2-pentanone (9%) and 3-pentanone (4%). Stockwell et al. (2015) deployed PTR-Time-of-Flight-mass spectrometer (PTR-TOF-MS) to measure the emissions from burning of large variety of biomass fuels and Muller et al. (2016) used instrumented (included PTR-TOF-MS) NASA aircraft for airborne sampling in a forest fire plume. The emission ratio (ER) of 2,3-butanedione with respect to acetonitrile reported by Karl et al. (2009) is 2.6 ± 3.1 ppbV/ppbV from laboratory studies and 1.9 ± 1.5 ppbV/ppbV from field studies, whereas the value reported by Muller et al. (2016) is 1.1 ppbV/ppbV. A recent study by our group (Sarkar et al., 2016), deployed PTR-TOF-MS to characterize the emissions from biomass burning and 2,3-butanedione was detected at $m/z = 87.042$ with average ambient mixing ratio of 0.35 ± 0.08 ppb. Another group estimated emissions of 2,3-butanedione from a biomass fire under non-turbulent nocturnal conditions using PTR-TOF-MS (Brilli et al., 2014). *Table 1.2.3* summarizes the emission factors (EF, g compound

emitted per kg dry fuel burned) of acetonitrile (biomass burning tracer) and 2,3-butanedione from different studies.

Emission factors (g/kg)	Andreae and Merlet (2001)	Yokelson et al. (2008)	Brilli et al. (2014)	Stockwell et al. (2015)	Müller et al. (2016)
Acetonitrile	0.18	0.49 ± 0.32	2.99	0.22 ± 0.17	0.19 ± 0.06
2,3-Butanedione	0.9	1.29 ± 0.82	6.17	1.15 ± 1.21	0.44 ± 0.18

Table 1.2.3: Emission factors (g/kg dry fuel) of acetonitrile and 2,3-butanedione

In this study, we quantify ambient concentration enhancements of 27 organic ions that were measured every minute using a proton transfer reaction mass spectrometer at IISER Mohali atmospheric chemistry facility during Feb 2013 – May 2013 covering the pre-wheat harvest and post-wheat harvest periods. The compounds were assigned based on careful consideration of their ambient time series and concentration profiles. Out of 27 compounds, 14 compounds were reported for the first time over N.W. IGP from wheat residue burning and those newly reported compounds are propyne, propene, formamide, formic acid, acrolein, methylketene, acetamide, acetic acid, nitromethane, hydroxyacetone, 2,3-butanedione, 2-furaldehyde, styrene and naphthalene. An attempt was made to understand the atmospheric chemistry of one of the newly reported VOC, i.e. 2,3-butanedione. Mann-Whitney U test was performed to determine the confidence interval (CI) at which the concentration of VOCs were significantly different between the pre-harvest and post-harvest season. An estimate of VOCs emitted (in Gg) from this activity was made using the emission ratio of VOCs to acetonitrile (biomass burning tracer) and the knowledge of CO emitted from this activity. Finally, the VOCs which majorly contributed to the total average reactive carbon, ozone formation potential and secondary organic aerosol formation potential were identified.

Chapter 2

2 Material and methods

2.1 Site description and criteria used for selection of durations of pre-harvest and post-harvest season

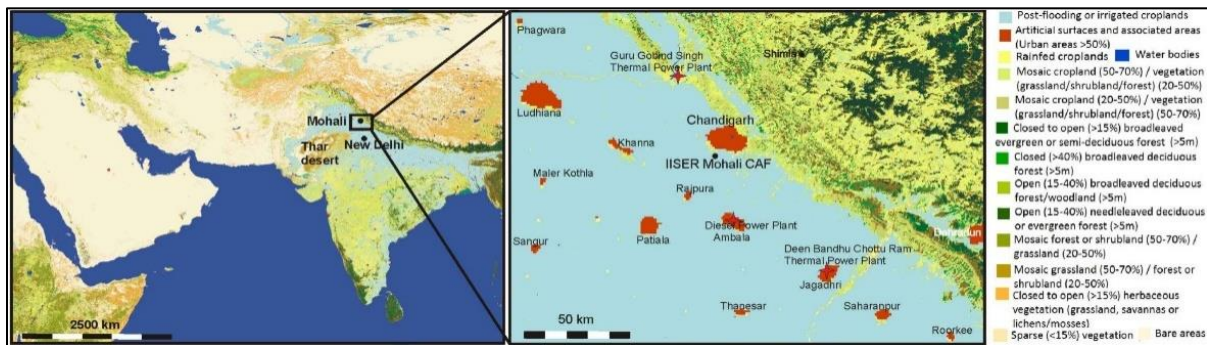


Figure 2.1.1: Left: Location of Mohali, in the NW-IGP. Right: Map of the land use in a 100 km×200 km area surrounding the measurement site (black dot, 30.667° N, 76.729°E, 310 m asl) (Sinha et al., 2014)

Error! Not a valid bookmark self-reference.(left) shows the location of the site in Mohali, super-imposed on a land-use map in the northwest Indo-Gangetic Plain close to the foothills of the Himalayan mountain range. The measurements were carried out at the atmospheric chemistry facility (30.667° N, 76.729°E, 310 m asl) of the Indian Institute of Science Education and Research (a sub-urban site in the city Mohali). **Error! Not a valid bookmark self-reference.**(right) shows the precise location of the measurement facility and its spatial relationship with respect to neighboring cities and the Himalayan mountain range. The

campus is mainly residential with tree cover and a few industrial units in the vicinity. A detailed description of the site including technical details pertaining to sampling, inlets and instrumentation and surrounding land use are available elsewhere (Sinha et al., 2014) (Pawar et al., 2015).

In the wind sector North to North-East of the measurement site, lie the cities of Mohali, Chandigarh and Panchkula. The Himalayan mountain range is less than 30 kms away in the north west to south-east direction. This sector is classified as urban sector due to the presence of urban emission sources. Industrial and rural sources lie in the wind sector spanning east to south. The wind sector spanning 90° - 180° is primarily mixed- rural and industrial in land use. Pharmaceutical industries, glass manufacturing units, solvent industries and paint industries are the major small scale industries present in this sector. About 300 km south of the site lies New Delhi, the capital of India. The wind sector spanning from South to North-West (180° - 315°) is dominated by agriculture activity and hence classified as rural and agricultural sector.

For the present analysis, we have characterized the period from 28 February to 30 April 2013 as not influenced by wheat residue fires termed “pre-wheat harvest”. The onset of the period influenced by wheat residue fires termed as “post-wheat harvest” is defined to be from 1 May to 31 May 2013. The duration for the pre and post wheat harvest period in the summer of 2013 was determined based on the following three criteria: 1) satellite derived fire count data, 2) ambient concentrations of acetonitrile (biomass burning tracer), 3) consistency of meteorological conditions and fetch region. The daily fire counts data over the region (red dots in black square box of *Figure 2.1.2*) were detected by the Moderate Resolution Imaging Spectroradiometer (MODIS) onboard two synchronous polar orbiting satellites called Aqua and Terra (MODIS:NASA/University of Maryland, 2002, MODIS Hotspot/Active Fire Detections Dataset, <http://maps.geog.umd.edu>). The Terra overpasses in the morning, generally between 10 am – 12 pm and the Aqua overpasses in the afternoon, generally between 1 – 3 pm.

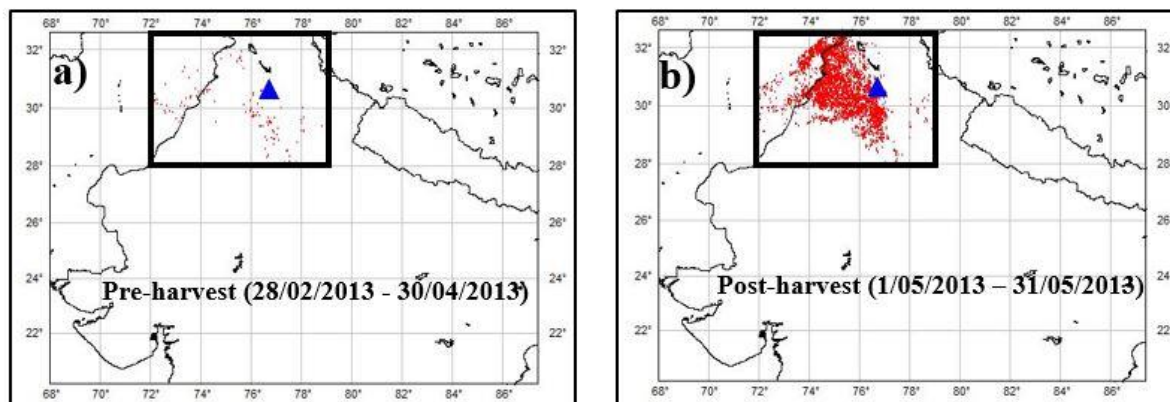


Figure 2.1.2: Total number of fire counts detected (at $\geq 80\%$ confidence interval) in 2013 by MODIS satellite over N.W.IGP (black square box) during (a) pre-wheat harvest period (28 February- 30 April 2013) and (b) post-wheat harvest period (1 May–31 May 2013). Blue triangle marks the location of the measurement site (30.667°N , 76.729°E , 310 m a.s.l.).

The major agricultural regions in the N.W. IGP between 28°N to 33°N and 72°E to 79°E is enclosed in the black square boxes in Figure 2.1.2 (a) and (b). This figure shows the spatial extent of open fires and the red dots show the total number of fire counts detected in the year 2013. *Figure 2.1.3* shows the daily fire counts detected using MODIS from 28 February to 30 April 2013 (pre-harvest period and shaded light blue) and from 1 May to 31 May 2013 (post-harvest period and shaded light pink). The total number of the open fires detected during the post-harvest season were 6231, whereas during the pre-harvest were only 434 (at a confidence interval of $\geq 50\%$). Significant enhancements were also observed in the mixing ratios of acetonitrile (biomass burning tracer) in the post-wheat harvest period. The average ambient concentration of acetonitrile in the pre-wheat harvest period was $0.72 (\pm 0.52)$ ppb whereas in the post-wheat harvest period was $1.38 (\pm 1.30)$ ppb. The fetch region during pre and post-wheat harvest period was predominantly from northwest direction of the site which is an agricultural land use area. While the exact date for the onset of wheat burning influenced period can be argued by 3-4 days but 1 May 2013 was chosen to be the onset of post-wheat harvest period as including or excluding few days does not change the scientific conclusions attained from this study.

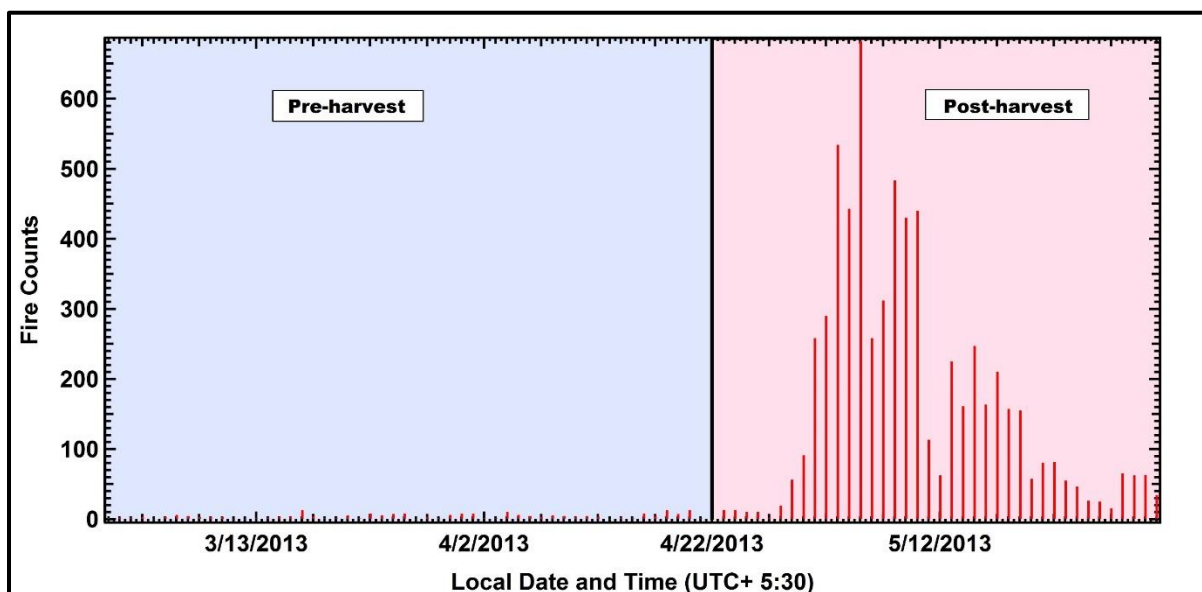


Figure 2.1.3: Daily fire counts detected by MODIS at confidence interval $\geq 50\%$ over N.W.IGP (28°N to 33°N and 72°E to 79°E) during the pre-wheat harvest (28 February-30 April 2013) and post-wheat harvest season (1-31 May 2013)

2.2 Prevalent meteorology

Wind speed, wind direction, relative humidity and ambient temperature were measured at a temporal resolution of 1 minute using meteorological sensors (Met One Instruments Inc., Rowlett, Texas, USA) at IISER Mohali Atmospheric Chemistry Facility. The wind rose plot for period of study (28/02/2013-31/05/2013) is shown in

Figure 2.2.1. *Figure 2.2.2* shows the diel profile of the relative humidity, ambient temperature, wind speed and solar radiation in the pre-wheat harvest and post-wheat harvest period along with their associated variability.

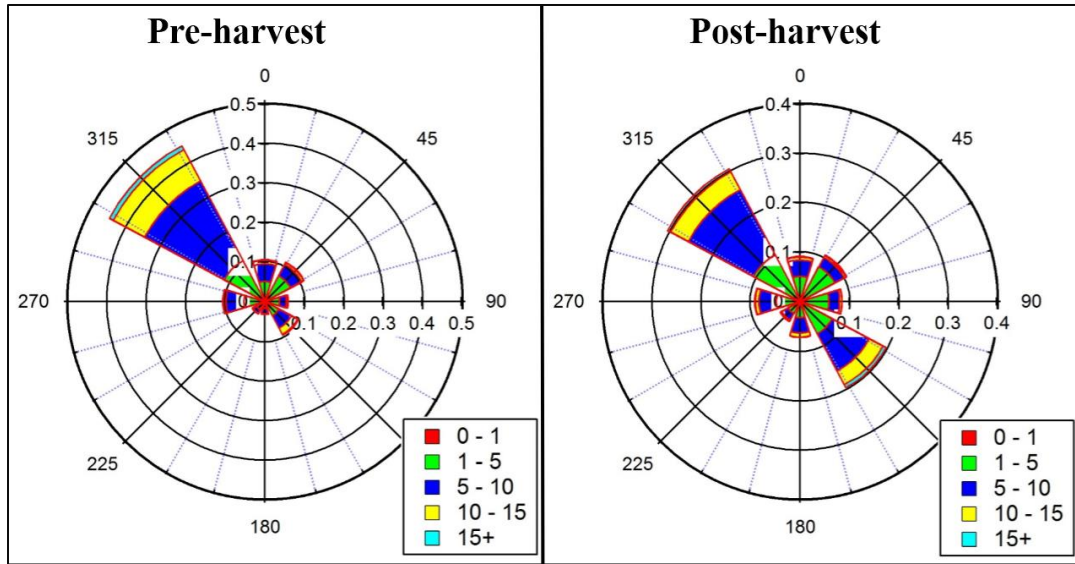


Figure 2.2.1: Wind rose plot for the measurement site (30.667N, 76.729 E, 310 m a.s.l.) for pre-harvest and post-harvest period

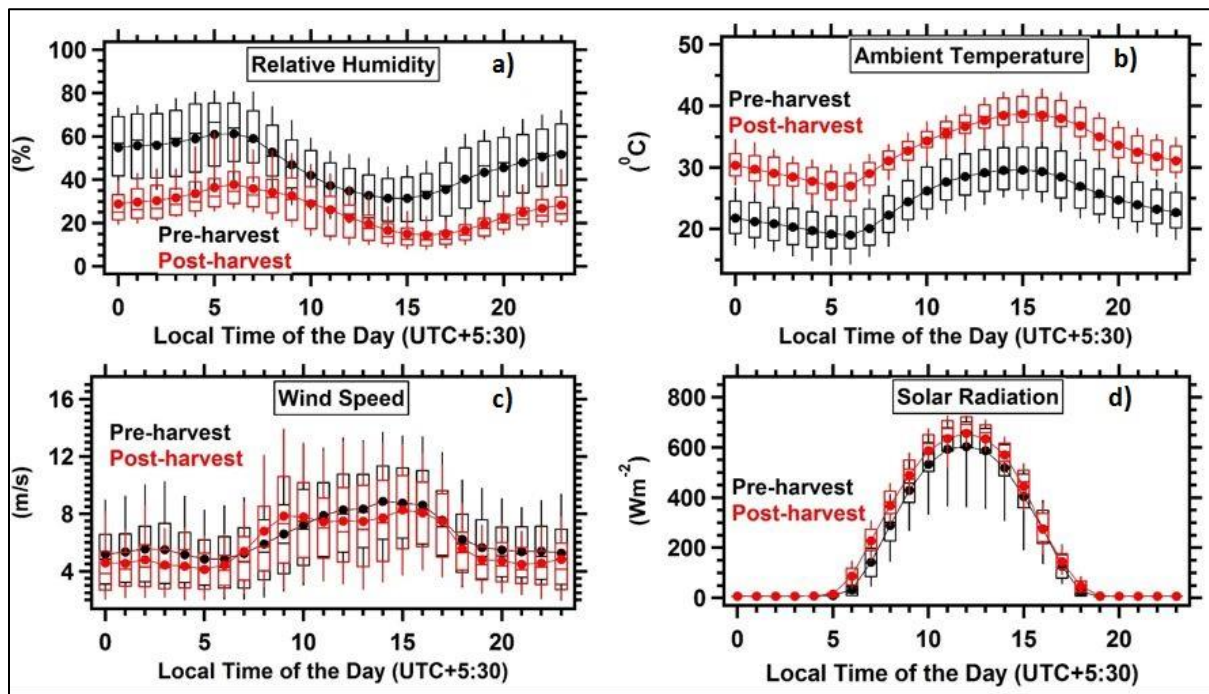


Figure 2.2.2: Diel profile of (a) relative humidity, (b) ambient temperature, (c) wind speed, and (d) solar radiation at the measurement site in the pre-wheat harvest ($n \geq 85650$)

measurements for each met parameter) and post-wheat harvest period ($n \geq 43510$ measurements for each met parameter). Markers represent hourly average and the top and bottom end of the box represents the 75th and 25th percentile, respectively. The vertical line in the middle of the box indicates the median whereas the whiskers represent the 90th and 10th percentile.

Table 2.2.1 summarizes the average of meteorological parameters during the pre-harvest and post-harvest period. The month of May is associated with warm and dry days in which day-time average solar radiation peaked at $\sim 660 \text{ Wm}^{-2}$ at 12:00 L.T. whereas in the months of February-April, the day-time average solar radiation peaked at $\sim 600 \text{ Wm}^{-2}$ at 12:00 L.T. The average ambient temperature was higher by a factor of $\sim 10^0\text{C}$ throughout the day in post-wheat harvest period in comparison to pre-wheat harvest. This could be due to the warming within the boundary layer from large-scale wheat residue fires in the month of May. This also points to more efficient boundary layer mixing that should result in lower post-harvest concentrations if only meteorology were the driving factor.

The average relative humidity was lower in the post-harvest by 20% in comparison to pre-harvest. In both the periods, the average wind speed was $5\text{-}6 \text{ ms}^{-1}$ and the fetch region was predominantly North West.

Parameters	Pre-wheat harvest (28/02/2013 - 30/04/2013)	Post-wheat harvest (01/05/2013 - 31/05/2013)
Ambient temperature ($^{\circ}\text{C}$)	24.4 (5.3)	33.0 (5.0)
Relative humidity (%)	46.6 (18.2)	26.1 (12.9)
Wind speed (m/s)	6.4 (3.4)	5.9 (3.4)
Most frequent wind direction	North West	North West

Table 2.2.1: Average ambient temperature, relative humidity, wind speed and most frequent wind direction during pre-wheat harvest and post-wheat harvest periods. The number in brackets correspond to $\pm 1\sigma$ ambient variability.

2.3 Volatile organic compound measurements using a proton transfer reaction mass spectrometer

In this study, a high-sensitivity proton transfer reaction quadrupole mass spectrometer (HS Model 11-07HS-088; Ionicon Analytik Gesellschaft, Austria) was used for online measurements of selected volatile organic compounds. This technique was developed by Professor Werner Lindinger and co-workers at the University of Innsbruck in Austria in 1998 (Lindinger et al., 1998). It works on the principle of soft chemical ionization (negligible/less fragmentation of product ion). The reagent ions (H_3O^+) perform non-dissociative proton transfer to VOCs which have a proton affinity (P.A.) greater than that of water (P.A. = 165.2 kcal/mol). It can quantify trace level VOCs (ppt range) in the ambient air and allows real time quantification of VOCs. A detailed description of the instrument used in this work has been provided in Sinha et al., 2014.

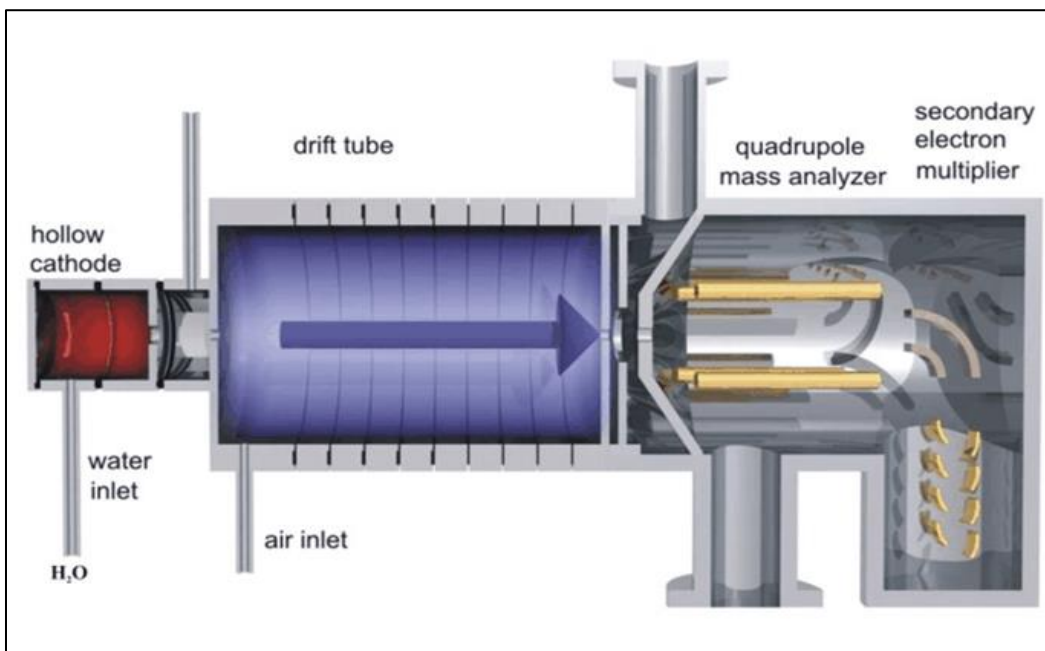
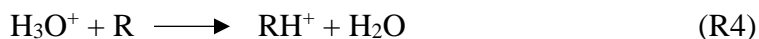


Figure 2.3.1: Schematic diagram of the proton transfer reaction mass spectrometer (PTR-MS) instrument

The instrument has four major parts as shown in *Figure 2.3.1*:

1. Hollow cathode ion source: Production of highly pure H_3O^+ (>95%) reagent ions takes place by plasma discharge of water vapor by application of 450 V DC voltage.
2. Drift-tube: Drift tube is made of stainless steel, separated by Teflon rings and resistors such that the potential across the entire drift tube length (~9.3 cm) is 600V. Inside the drift tube, soft chemical ionization of analyte molecules with proton affinity greater than that of water (e.g. VOCs) takes place as



where R is any analyte molecule and RH^+ is the protonated molecular ion.

3. Quadrupole mass analyzer: It separates the protonated molecular ions according to their mass/charge (m/z) ratio.
4. Secondary electron multiplier: It is used to detect the ion signal. The typical operating pressure for the detection region is 10^{-5} mbar.

The inlet used for PTR-MS is made up of opaque Teflon tubing with inlet diameter of 3.12 mm and about 12 m in length. It is located at the top of air quality station which is at a height of ~20m agl but the instrument itself is installed in a room on the first floor of Central Analytical Facility (CAF) building.

2.4 Data quality assurance

2.4.1 Calibration procedure

To determine the sensitivity and limit of detection provided by PTR-MS for aromatic VOCs, calibrations were performed wherein high purity VOC calibration gas at different flows was introduced after dynamically diluting it with a constant flow of VOC free zero air. Zero air

was generated by passing synthetic zero air (Sigma gases; 99.9999% purity) over a Supelco activated charcoal tube and VOC scrubber catalyst (Gas calibration unit; Ionimed Analytik, Innsbruck, Austria, (Sinha et al., 2014)). PTR-MS signal observed while passing zero air was taken as the instrumental background. The ion signal obtained from PTR-MS in counts per second (cps) was then converted into normalized counts per second (ncps) using the following equation (Sinha et al., 2009):

$$\text{ncps} = \frac{I(\text{RH}^+) \times 10^6}{I(\text{H}_3\text{O}^+) + I(\text{H}_3\text{O}^+(\text{H}_2\text{O}))} \times \frac{2}{p_{\text{drift}}} \times \frac{T_{\text{drift}}}{298.15}. \quad (2)$$

The measured ion signals were normalized with respect to both hydronium ions (H_3O^+ ; $m/z = 19$) and hydrated hydronium ion water clusters ($\text{H}_3\text{O}^+(\text{H}_2\text{O})$; $m/Z=37$). The sensitivity factors (ncps ppb^{-1}), i.e., the slope of linear fit of measured response (ncps) versus introduced mixing ratio (ppb) were derived from the calibration plots. These sensitivity factors were then used to convert normalized counts per second to ppb for all the VOCs reported in this work. The calibration plots for selected VOCs are shown in *Figure 2.4.1*. These calibration plots showed an excellent linearity over the entire dynamic range. The horizontal error bars represent the root mean square propagation of errors due to error in gas standards (6% each for benzene and toluene, 5% each for p-xylene and 1,2,4-trimethylbenzene) and 2% each error for the two mass flow controllers used during calibration. The vertical error bars represent 2σ instrumental precision error while sampling the standard gas at each dilution point. The total uncertainty was given as root mean square of accuracy error and precision error.

$$\text{Total uncertainty} = \sqrt{[(\text{accuracy error})^2 + (\text{precision error})^2]} \quad (3)$$

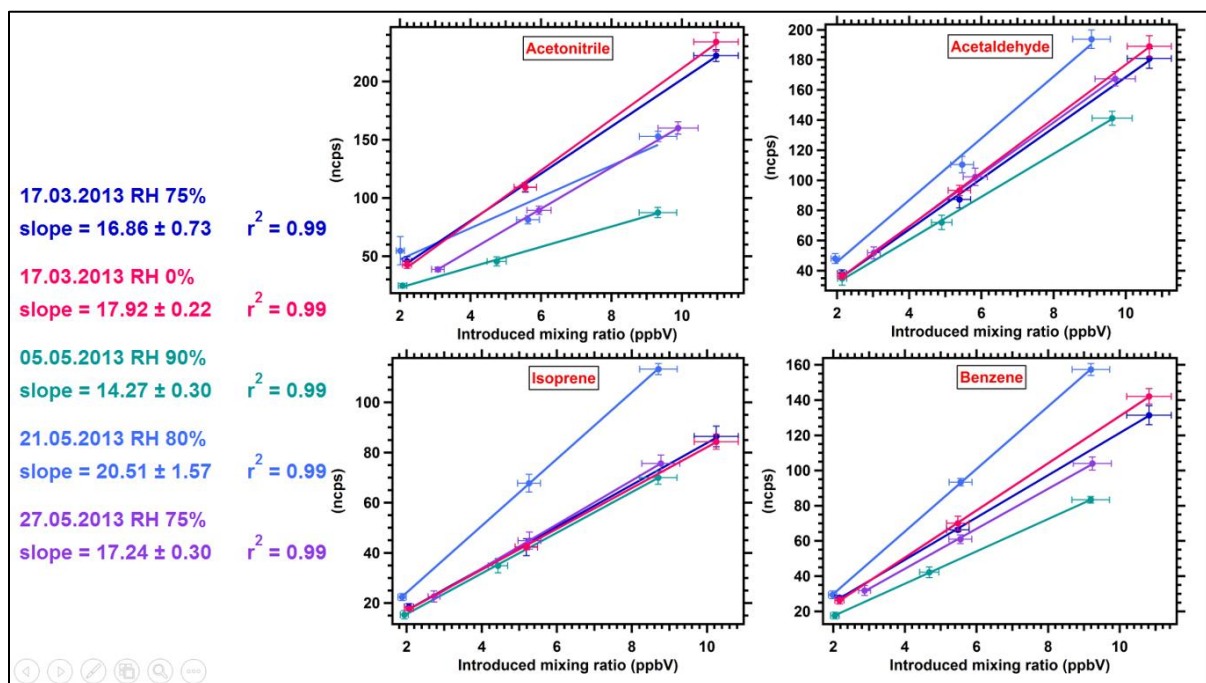


Figure 2.4.1: Sensitivity and linearity of selected VOCs (acetonitrile, acetaldehyde, isoprene and benzene) in the calibration experiment performed on 17/03/2013 at RH 0% (shown in pink) and RH 75% (shown in blue), 05/05/2013 at RH 90% (shown in green), 21/05/2013 at RH 80% (shown in light-blue) and 27/05/2013 at RH 75% (shown in purple). The y-axis represents the PTR-MS response in normalized counts per second (ncps) and the x-axis represents the introduced mixing ratio in ppb. The vertical bars in the figure represent the 2σ precision error of the measurements whereas the horizontal bars represent the error due to the uncertainty in the VOC gas standard and flow reproducibility of two MFCs.

Table 2.4.1 lists the VOC m/z assignments, molecular formula, sensitivity, limit of detection and total uncertainty for VOCs reported in this study. Figure 2.4.2 shows the calibration factors (ncps/ppb) for PTR-MS versus mass of the calibrated species. Sensitivity factors for all the observed masses where direct calibrations were not available were deduced using the quadratic fit (solid purple line).

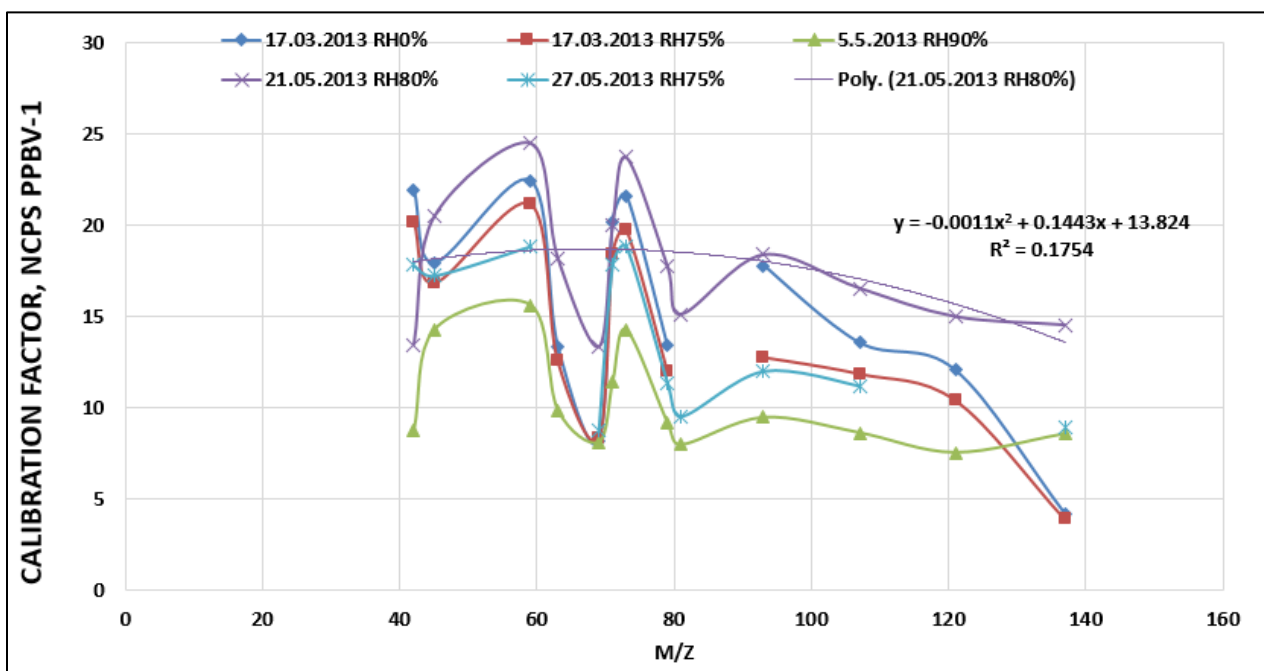


Figure 2.4.2: Calibration factors (ncps/ppb) for PTR-MS vs mass of the calibrated species which are acetonitrile, acetaldehyde, acetone, dimethyl sulfide, isoprene, methyl vinyl ketone, methyl ethyl ketone, benzene, toluene, p-xylene, 1,2,4-trimethylbenzene and monoterpenes. The calibration factors were obtained from various calibration experiments performed at different relative humidities. The dates of various calibration experiments are: 17/03/2013 at RH 0% (light blue markers) and RH 75% (red markers), 05/05/2013 at RH 90% (olive green markers), 21/05/2013 at RH 80% (purple markers) and 27/05/2013 at RH 75% (aqua markers). Calibration factors for all the observed masses where direct calibrations were not available were deduced using the quadratic fit (solid purple line).

VOC	Nominal protonated m/z	Formula	Sensitivity (ncps/ppbV)	Limit of detection (ppbV)	Uncertainty (%)
Methanol	33	CH ₃ OH	17.4	0.43	8.9 %
Propyne	41	C ₃ H ₄	17.9	0.06	~50 %
Acetonitrile	42	CH ₃ CN	13.4	0.07	8.7 %
Propene + fragment of acetic acid	43	C ₃ H ₆	17.9	0.32	~50 %
Isocyanic acid	44	NHCO	18.0	0.09	~50 %
Acetaldehyde	45	C ₂ H ₄ O	20.5	0.17	8.6 %
Formamide	46	CH ₃ NO	18.1	0.18	~50 %
Formic acid + Ethanol	47	CH ₂ O ₂ + C ₂ H ₆ O	18.2	0.29	~50 %
Acrolein + Methylketene	57	C ₃ H ₄ O	18.5	0.06	~50 %
Acetone	59	C ₃ H ₆ O	24.5	0.11	8.4 %
Acetamide	60	C ₂ H ₅ NO	18.5	0.12	~50 %
Acetic acid	61	C ₂ H ₄ O ₂	18.5	0.15	~50 %
Nitromethane	62	CH ₃ NO ₂	18.5	0.05	~50 %
Dimethyl Sulfide	63	C ₂ H ₆ S	18.2	0.11	8.1 %
Isoprene	69	C ₅ H ₈	13.3	0.09	7.6 %
Methyl vinyl ketone	71	C ₄ H ₆ O	19.9	0.04	9.3 %
Methyl ethyl ketone	73	C ₃ H ₄ O ₂	23.7	0.06	8.6 %
Hydroxyacetone	75	C ₃ H ₆ O ₂	18.5	0.06	~50 %
Benzene	79	C ₆ H ₆	17.8	0.03	7.9 %
Assorted Hydrocarbons	83	C ₆ H ₁₀	18.2	0.04	~50 %
2,3-Butanedione	87	C ₄ H ₆ O ₂	18.1	0.09	~50 %
Toluene	93	C ₇ H ₈	18.4	0.07	8.3 %
2-Furaldehyde (furfural)	97	C ₅ H ₄ O ₂	17.5	0.07	~50 %
Styrene	105	C ₈ H ₈	16.8	0.06	~50 %
Xylenes	107	C ₈ H ₁₀	16.5	0.07	9.9 %
Trimethylbenzenes	121	C ₉ H ₁₂	14.9	0.03	8.3 %
Naphthalene	129	C ₁₀ H ₈	14.1	0.07	~50 %

Table 2.4.1: Compound-specific VOC m/z assignments, nominal protonated m/Z ratios, sensitivity, limit of detection and uncertainty

Hence, PTR-MS provides accurate measurements of VOCs in the ambient air offering rapid response time and excellent detection limits. For this study, we used aromatic VOC measurements performed at a temporal resolution of 1 min during February-May 2013.

Calibration factors for all the observed masses where direct calibrations were not available were deduced using the quadratic fit (solid purple line) in *Figure 2.4.2*. Theoretically, the sensitivity factor can be calculated using the following equation (de Gouw et al., 2003):

$$\text{Sensitivity} = 10^{-3} \times \frac{kL}{\mu_0 N_0} \times \frac{N^2}{E} \times \frac{T(\text{RH}^+)}{T(\text{H}_3\text{O}^+)} \quad (4)$$

where,

k = rate coefficient for proton-transfer reaction

L = length of drift-tube (9.3 cm)

μ_0 = ion mobility of H_3O^+

N_0 = gas number density at STP

N = number density of the gas in drift tube

E = electric field in the drift tube

$T(\text{RH}^+)$ = transmission efficiency for RH^+

$T(\text{H}_3\text{O}^+)$ = transmission efficiency for H_3O^+

The sensitivity factors of the calibrated species obtained from calibration experiments were compared with the sensitivity factors obtained theoretically using the above equation and the uncertainty was less than 30 %. For the VOCs not present in the gas standard, the sensitivity factors obtained using the quadratic fit (solid purple line in *Figure 2.4.2*) were compared with the theoretically calculated sensitivity factors and the uncertainty was less than 40 %.

2.4.2 Data Quality Assurance to exclude local pollution events

The influences on the measurements from very local emissions sources such as residences, hostel emissions and buildings are expected to be significant at low wind speeds. Therefore, in order to minimize the influence of very local events, time-periods with wind speed $< 1\text{ms}^{-1}$ (calm conditions) were filtered out for the analysis carried out in this work. This resulted in exclusion of about 3.3% of the data and data pertaining to periods with wind speed $\geq 1\text{ms}^{-1}$ i.e. 96.7 % of the dataset was considered for further analyses.

Chapter 3

3 Results and discussion

3.1 Identification of rarely measured VOCs in the summer time air of NW-IGP

The PTR-MS deployed in this study was operated in the ion-selective monitoring mode (in the mass range 21-183 amu). The compounds were assigned based on careful consideration of following factors (Sarkar et al., 2016):

1. For the attribution of peaks only to the VOCs present in the ambient air and not due to instrumental noise, a 200 ppt cut-off for VOC concentrations was fixed, i.e., only those VOCs which had an average concentration ≥ 200 ppt were considered for the analysis. The 200 ppt cut off was chosen as an additional quality control measure since the instrumental backgrounds can be as high as 170 ppt at certain m/z channels.
2. Next, a rigorous investigation of the time series of each compound was done and the compounds which showed no ambient variation in the diel profile were ruled out from compound assignment.
3. A methodical comparison between the diel profile of rarely measured VOCs and that of VOCs measured routinely using PTR-MS, for example acetonitrile, benzene, isoprene, acetaldehyde and toluene was done for constraining their emission sources.

Using this algorithm, 27 protonated organic ions were identified and a complete list of these organic ions is given in Table 2.4.1 and their most plausible chemical structures are shown in *Figure 3.1.1*.

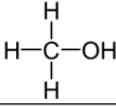
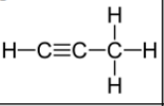
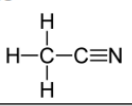
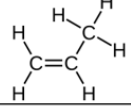
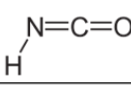
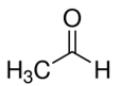
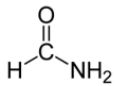
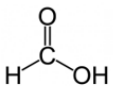
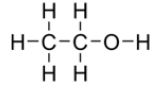
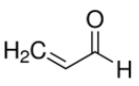
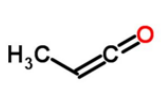
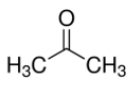
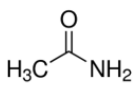
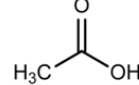
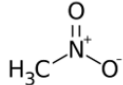
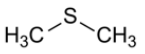
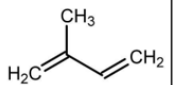
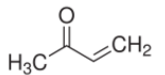
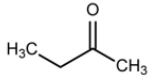
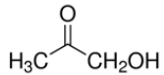
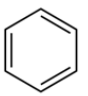
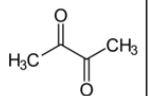
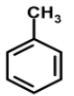
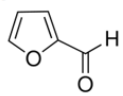
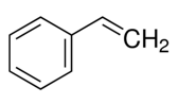
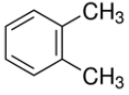
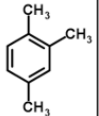
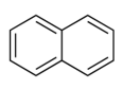
Methanol 	Propyne 	Acetonitrile 	Propene 	Isocyanic acid 
Acetaldehyde 	Formamide 	Formic acid 	Ethanol 	Acolein 
Methylketene 	Acetone 	Acetamide 	Acetic acid 	Nitromethane 
Dimethyl Sulfide 	Isoprene 	Methyl vinyl ketone 	Methyl ethyl ketone 	Hydroxyacetone 
Benzene 	2,3-Butanedione 	Toluene 	2-Furaldehyde 	Styrene 
Xylene 	Trimethyl benzene 	Naphthalene 		

Figure 3.1.1: Chemical structure of VOCs identified in this work

3.2 Chemistry of 2,3-butanedione

Figure 3.2.1 shows the time series of the ambient concentrations (1minute resolution data) for acetonitrile (biomass burning tracer) and 2,3-butanedione during the pre-wheat harvest (28 February - 30 April 2013) and post-wheat harvest period (1 May - 31 May 2013). It is quite evident from the time series plot that the ambient concentrations of acetonitrile and 2,3-butanedione increased in the post-wheat harvest season in comparison to the pre-wheat harvest season. The average concentrations of acetonitrile and 2,3-butanedione in pre-harvest

season were 0.72 ± 0.52 ppb and 1.25 ± 0.57 ppb, respectively and in post-harvest season were 1.35 ± 1.30 ppb and 2.35 ± 1.08 ppb, respectively. Therefore, the average concentrations of acetonitrile and 2,3-butanedione were higher by a factor of 1.87 and 1.88, respectively in the post-harvest period relative to pre-harvest period. The data break from 02/04/2013-22/04/2013 is due to OH reactivity experiment (Kumar and Sinha, 2014). The gaps in the data during 29/04/2013 - 04/05/2013 was due to calibration and maintenance of PTR-MS instrument.

Figure 3.2.2 shows the time series of 2,3-butanedione and solar radiation in Watts/m² from 23/04/2013 - 26/04/2013 clearly indicating its night-time direct emissions (primary source) and its day-time photochemical production (secondary source) at our site.

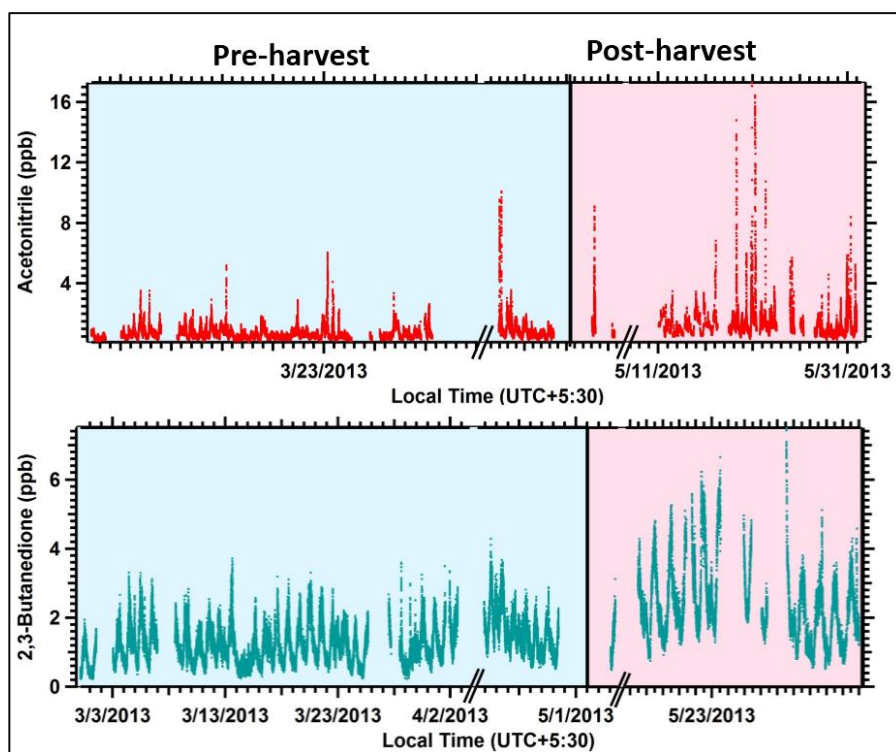


Figure 3.2.1: Time series of one-minute data for the ambient concentrations of acetonitrile (top panel) and 2,3-butanedione (bottom panel) in pre-wheat harvest (shown in pale blue region) and post-wheat harvest period (shown in pale pink region).

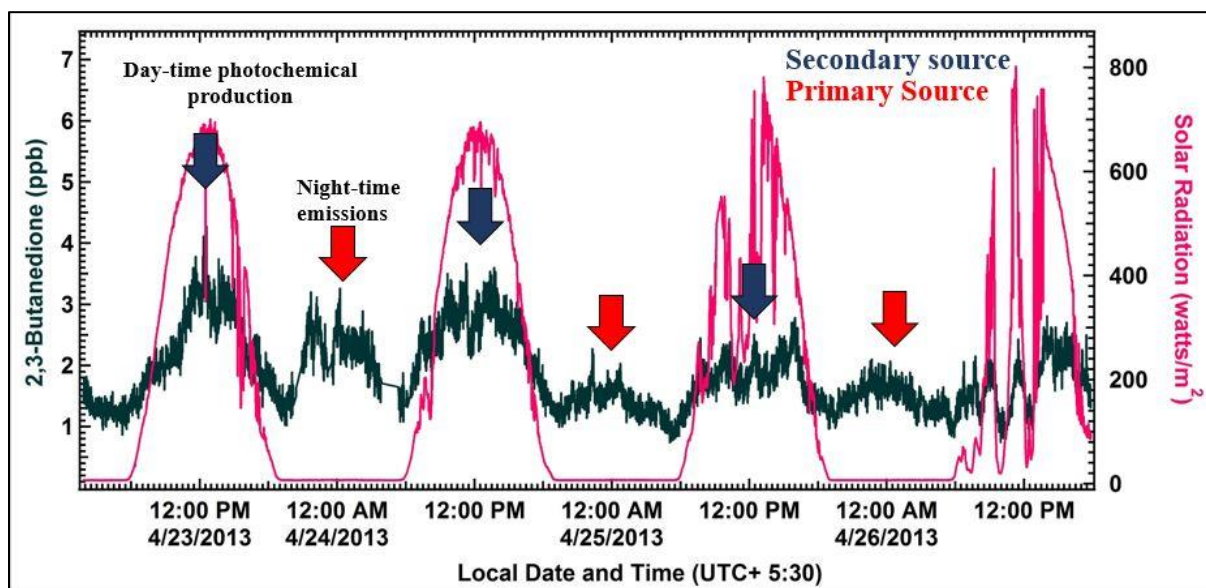


Figure 3.2.2: Time series of mixing ratio of 2,3-butanedione (dark green) and solar radiation in Watts/m² (pink) from 23/04/2013-26/04/2013. The red arrow indicates the night-time direct emissions of 2,3-butanedione (primary source) and the blue arrow indicates its day-time photochemical production (secondary source).

The compound 2,3-butanedione is formed photochemically and its known precursors are trimethylbenzenes, o-xylene methyl ethyl ketone (MEK). The diel box and whisker plots for the precursors of 2,3-butanedione during pre-wheat harvest and post-wheat harvest season are shown in the Figure 3.3.1. The reaction of methyl ethyl ketone with hydroxyl radicals to form 2,3-butanedione is an aqueous phase reaction. Usually, the relative humidity is low (~40%) in the summer time and hence the conditions for the formation of 2,3-butanedione from MEK are not conducive. The yield of 2,3-butanedione was determined from the slope of the its correlation plots with C-8 aromatics and C-9 aromatics (precursors of 2,3-butanedione) as shown in Figure 3.3.1. Only the day time hourly averaged concentrations were considered as it is formed photochemically from C-8 aromatics and C-9 aromatics. No significant enhancements in ambient concentrations of C-8 aromatics due to post-harvest wheat residue fires and its negative correlation with 2,3-butanedione suggests that C-8 aromatics are not the

likely precursors. The yield from C-9 aromatics (sum of isomers of trimethylbenzene) is $79 \pm 8 \%$, which is much higher than the yields reported by other chamber studies (*Table 1.2.1*). Also, the ambient concentrations of C-9 aromatics were 3 times higher during post-harvest period relative to pre-harvest period. This suggests that C-9 aromatics are the more likely precursors of 2,3-butanedione at our site, but there must certainly be more precursors.

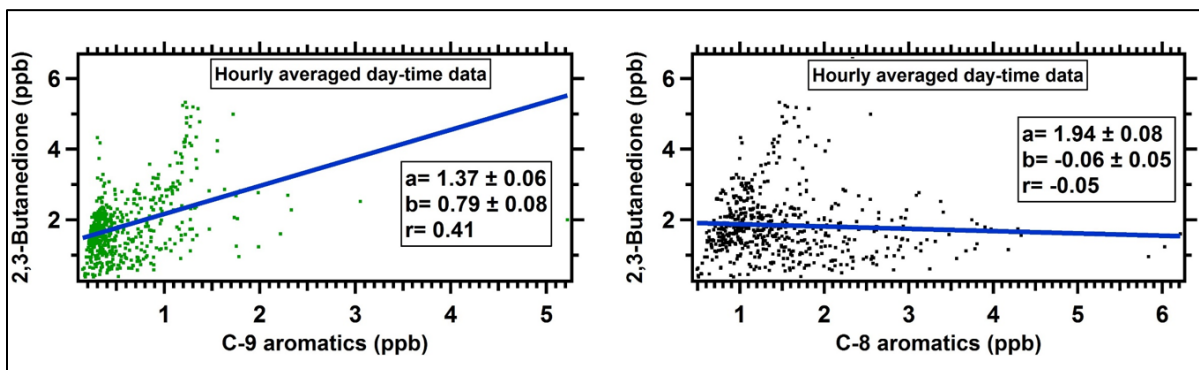
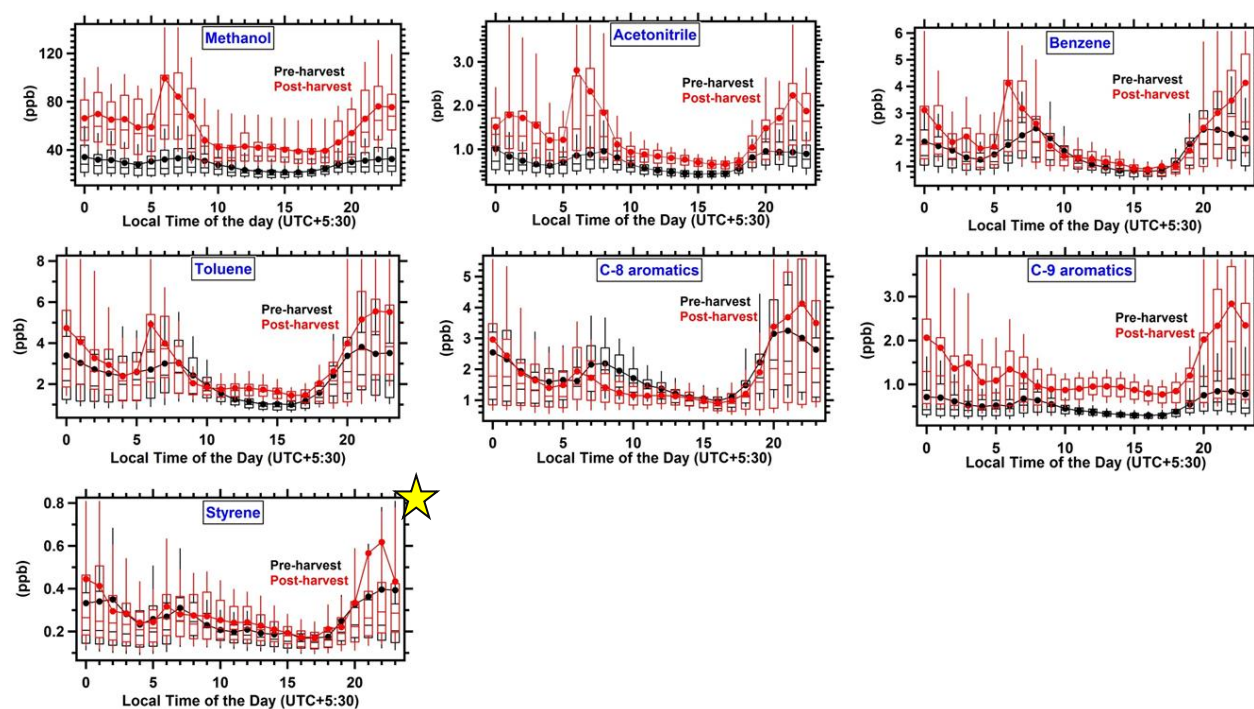


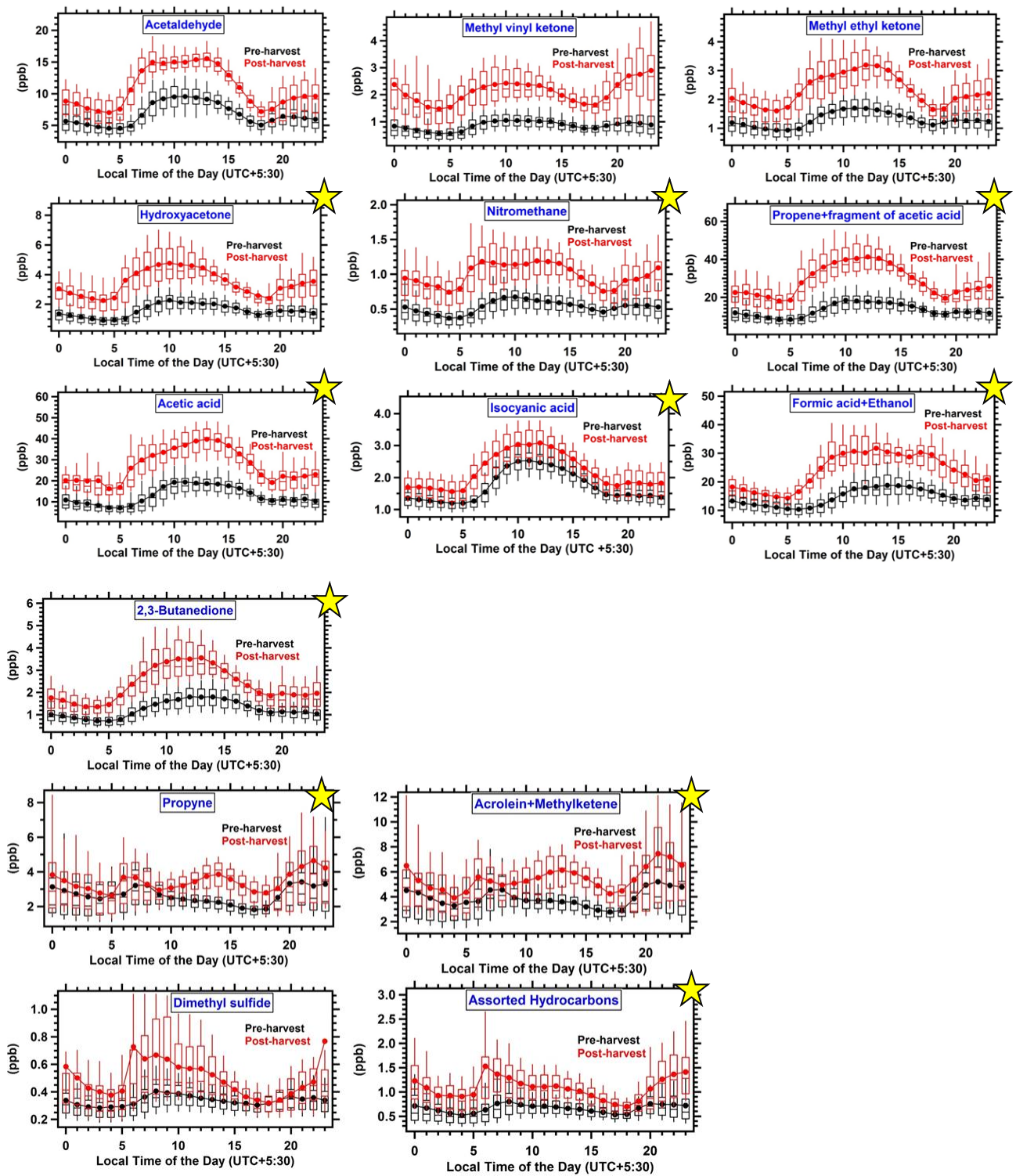
Figure 3.2.3: Correlation plot of 2,3-butanedione with C-9 aromatics (left) and C-8 aromatics (right). Individual data points in these plots are daytime hourly averaged mixing ratios (06:00 to 18:00 L.T.). Solid lines (shown in blue) are the linear regression fits through these data points and the regression equations and correlation coefficients are also indicated in the plots.

3.3 Diel variability of VOCs during pre-harvest and post-harvest periods

Figure 3.3.1 shows the diel box and whisker plot for mixing ratios of frequently quantified VOCs which are: methanol, acetonitrile, acetaldehyde, acetone, dimethyl sulfide, isoprene and furan, benzene, methyl vinyl ketone, methyl ethyl ketone, toluene, C-8 aromatics (sum of xylenes and ethylbenzene) and C-9 aromatics (sum of isomers of trimethylbenzene) during the pre-harvest (shown in black color; derived from total number of measurements, $n \geq 47504$ for each species) and post-harvest period (shown in red color; derived from total

number of measurements, $n \geq 17260$ for each species). It also shows the diel box and whisker plot for mixing ratios of rarely measured VOCs which are: propyne ($m/z = 41$), propene + fragment of acetic acid ($m/z = 43$), isocyanic acid ($m/z = 44$), formamide ($m/z = 46$), formic acid + ethanol ($m/z = 47$), acrolein + methylketene ($m/z = 57$), acetamide ($m/z = 60$), acetic acid ($m/z = 61$), nitromethane ($m/z = 62$), hydroxyacetone ($m/z = 75$), assorted hydrocarbons ($m/z = 83$), 2,3-butanedione ($m/z = 87$), 2-furaldehyde ($m/z = 97$), styrene ($m/z = 105$) and naphthalene ($m/z = 129$) during the pre-harvest (shown in black color; $n = 47507$ for each species where n = number of measurements) and post-harvest period (shown in red color; $n \geq 14391$ for each species).





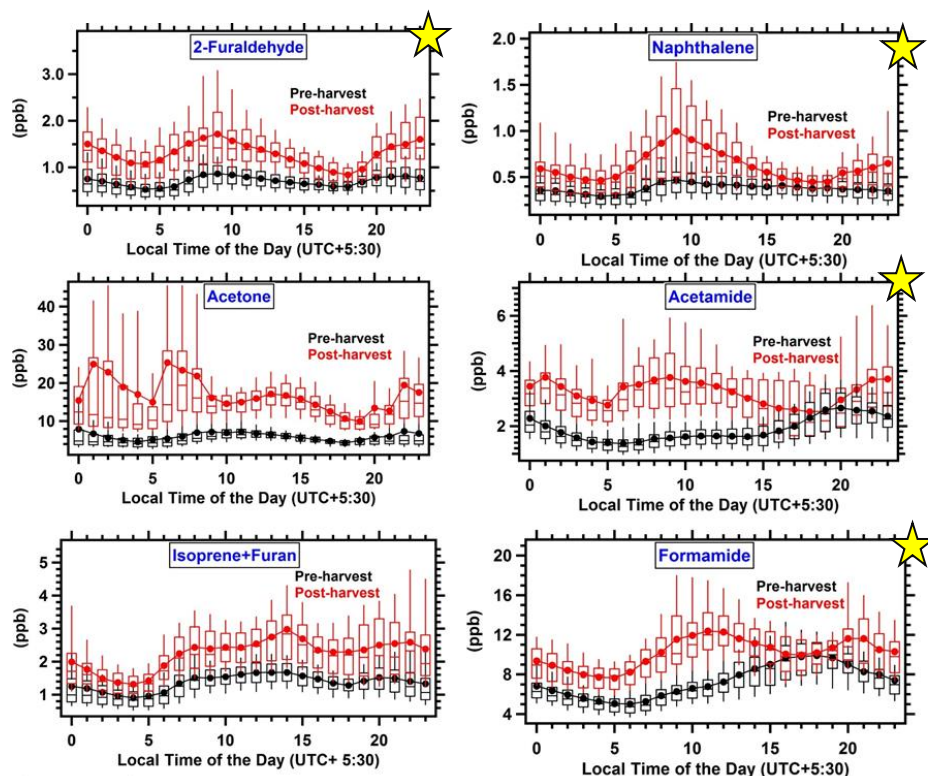


Figure 3.3.1: Diel box and whisker plot for mixing ratios of frequently quantified VOCs and rarely measured VOCs (star marked) during the pre-harvest (shown in black color) and post-harvest period (shown in red color).

Acetonitrile, methanol, benzene, toluene, C-8 aromatics, C-9 aromatics and styrene have a typical bimodal profile with a daytime minima and early morning and evening peak. During day-time, the observed diel decrease is primarily due to the effective dilution by elevated boundary layer (~1500-2500m) and also due to chemical loss processes. During night time, biomass burning and traffic emissions into a shallow nocturnal boundary layer (~50-100m) result in higher concentrations of VOCs. The average concentrations of acetonitrile and methanol were twice as high during the evening and night hours in the post-wheat harvest period relative to the pre-wheat harvest period. The maxima of the diel concentrations was attained around 06:00 LT as the concentrations were three times higher for both the compounds in post-harvest period relative to pre-harvest period. The minimum

concentrations were observed around 16:00 h but even during this time, the average concentrations of acetonitrile and methanol in the post-harvest period exceeded by 200 ppt and 17 ppb, respectively than those in the pre-harvest period. The diel profile of benzene and toluene suggests its strong early morning and nighttime emissions. On the other hand, strong nighttime emissions and weak daytime emissions were observed for C-8 aromatics, C-9 aromatics and styrene. The maxima of the diel concentrations was observed during the night hours (19:00-23:00 L.T.). The ambient concentrations of C-9 aromatics were 3 times higher in the nighttime hours during post-harvest period relative to pre-harvest period.

Isocyanic acid, acetic acid, propene and 2,3-butanedione have a characteristic photochemical profile with a daytime maxima and nighttime minima. A clear diurnal variation of these VOCs during both pre-harvest and post-harvest period suggests the presence of strong photochemical source. The concentrations of propene ($m/z = 43$) should be taken as the upper limit as in PTR-MS, protonated acetic acid loses a water molecule and forms a stable acetyl fragment ion (CH_3CO^+) which lands at $m/z = 43$ (Maleknia et al., 2007). Typical fragmentation for acetic acid is m/z 61+: 75% and m/z 43+: 25% (Karl et al., 2007). *Figure 3.3.2 (a)* shows the correlation plot of mass channel 43 (propene) with acetic acid ($m/z = 61$). The slope of linear regression fit is 0.84 and a strong correlation ($r = 0.98$) is observed. Therefore, propene ($m/z = 43$) was corrected for the fragmentation from acetic acid and the corrected diel box and whisker profile of propene during pre-harvest and post-harvest period is shown in *Figure 3.3.2 (b)*. The correction does not seem to have worked well, as propene still shows a photochemical profile.

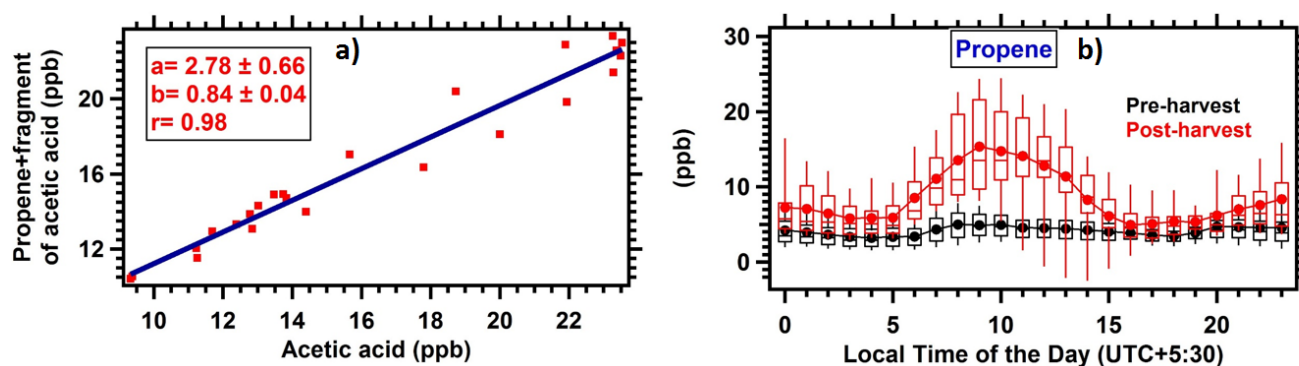


Figure 3.3.2: (a) Correlation plot of mass channel 43 (propene + fragment of acetic acid) with acetic acid. Data points in these plots are the hourly average concentrations. Solid line (shown in blue) is the linear regression fit through these data points and the regression equation and correlation coefficient are also indicated in the plot; (b) Diel box and whisker profile of propene (after correction) during pre-harvest and post-harvest period.

The diel profile of acetaldehyde, methyl vinyl ketone, methyl ethyl ketone, hydroxyacetone and nitromethane suggests strong daytime photochemical production of these VOCs. A secondary peak between 19:00 – 24:00 LT is also observed in the diel profile of these VOCs pointing to their direct emissions from biomass burning activities during nighttime.

The compounds like propyne and acrolein have a unique trimodal profile in the post-harvest period and bimodal profile in the pre-harvest period.

3.4 Statistical tests for assessing significance of difference in the ambient concentration of VOCs during pre-harvest and post-harvest periods

Mann-Whitney U test for equal medians was used to determine whether the differences in VOC concentrations during pre-harvest and post-harvest periods were statistically

significant. It is a non-parametric test to check whether the medians of two independent datasets are significantly different. The null hypothesis for this test is:

H_0 : The two samples (pre-harvest dataset and post-harvest dataset) for VOC are taken from populations with equal medians.

Serial No.	VOCs (daytime dataset)		Degree of enhancement	CI	Strongest emission
1	Acetone		>3 times	99.99 %	<div>Decreasing rank of emissions</div>
2	C-9 aromatics		2.5-3 times	99.99 %	
3	Methanol	Acetonitrile	2-2.5 times	99.99 %	
	MVK	Acetic acid			
	Nitromethane	Hydroxyacetone			
	Propene + fragment of acetic acid				
4	Acetaldehyde	Assorted Hydrocarbons	1.5-2 times	99.99 %	
	DMS	2,3-Butanedione			
	Isoprene	Naphthalene			
	MEK	2-Furaldehyde			
	Propyne	Formic acid + Ethanol			
	Formamide	Acrolein + Methylketene			
5	Benzene	Toluene	1-1.5 times	99.99 %	
	Isocyanic acid	Styrene			

Table 3.4.1: Results of Mann-Whitney U test for the daytime data (CI: Confidence Interval).

Serial No.	VOCs (nighttime dataset)		Degree of enhancement	CI	Strongest emission
1	Acetone	C-9 aromatics	>3 times	99.99 %	<div>Decreasing rank of emissions</div>
2	Methanol	Acetic acid	2-2.5 times	99.99 %	
3	MVK	Hydroxyacetone	1.5-2 times	99.99 %	
	Acetonitrile	Acetaldehyde			
	DMS	Isoprene			
	Nitromethane	2,3-Butanedione			
	2-Furaldehyde	Naphthalene			
	MEK	Propene + fragment of acetic acid			
	Assorted Hydrocarbons				
	Formic acid + Ethanol				
4	Benzene	Toluene	1-1.5 times	>99.9 %	
	Propyne	Isocyanic acid			
	Formamide	Acetamide			
	Acrolein + Methylketene	Styrene			
5	C-8 aromatics		1.2 times	95.45 %	

Table 3.4.2: Results of Mann-Whitney U test for the nighttime data (CI: Confidence Interval).

For the present analysis, hourly averaged data for VOC concentrations was taken and it was further divided into daytime (06:00 to 18:00 LT) and nighttime (18:00 to 06:00 LT). The pre-harvest daytime data ($n \geq 415$ measurements for each species) of all the reported VOCs was compared with the post-harvest daytime data ($n \geq 120$ measurements for each species). *Table 3.4.1* shows the confidence interval (CI) at which the concentration of VOCs were statistically different between the pre-harvest and post-harvest season during daytime. The table also shows the degree of enhancement (ratio of average post-harvest concentration to average pre-harvest concentration) in VOC concentrations during post-harvest season relative to pre-harvest season. A similar analysis was done for the nighttime data ($n \geq 400$

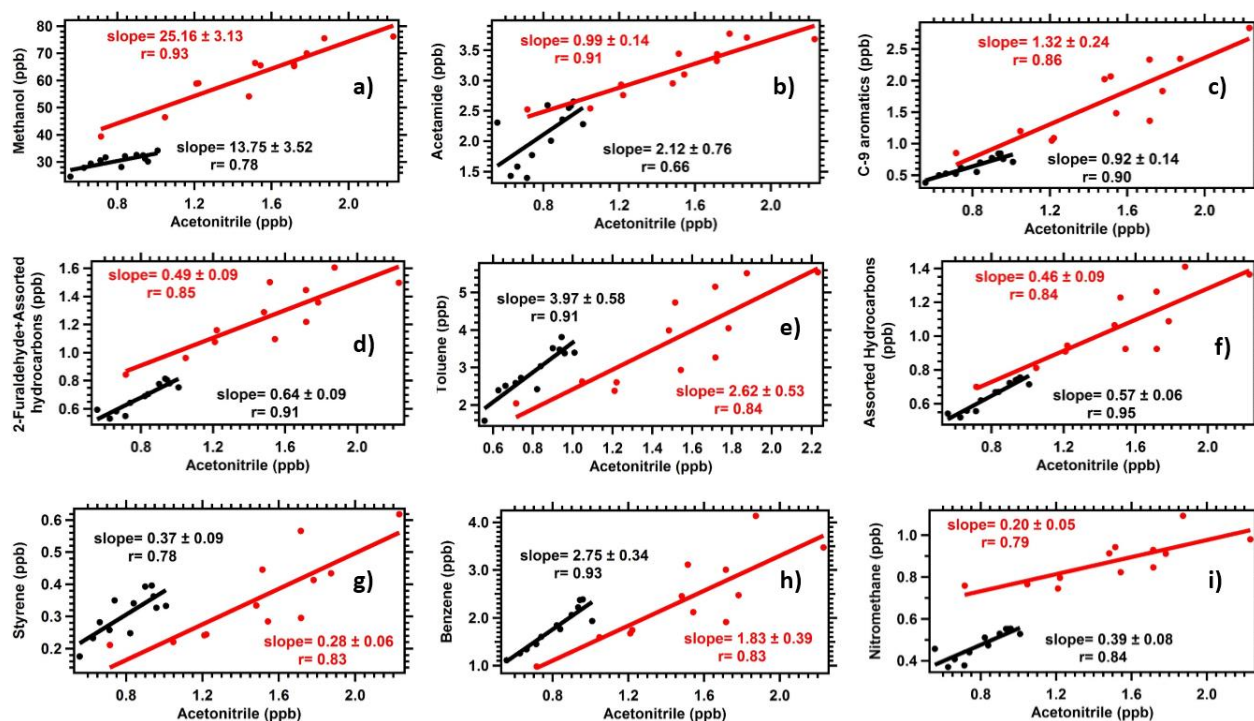
measurements for each species in pre-harvest and $n \geq 125$ measurements for each species in post-harvest) and the results are summarized in *Table 3.4.2*.

The pre-harvest and post-harvest concentrations of all VOCs were significantly different at a confidence interval of $>95.45\%$ (2σ) for the nighttime dataset. Infact for the nighttime dataset, 26 out of 27 compounds were statistically different at a confidence interval as high as 99.99% (4σ). Pre-harvest dataset of C-8 aromatics was not significantly different from values of post-harvest season for the daytime. Among all the VOCs, acetone and C-9 aromatics showed a high degree of enhancement in post-harvest period relative to pre-harvest period (~ 3 times enhancement). Throughout the day, the concentrations of methanol, acetic acid, methyl vinyl ketone and hydroxyacetone were 2-2.5 times higher, whereas the concentrations of acetaldehyde, DMS, isoprene, methyl ethyl ketone, 2,3-butanedione, naphthalene, 2-furaldehyde and formic acid were 1.5-2 times higher during post-harvest period relative to pre-harvest period. The degree of enhancement for aromatics such as benzene, toluene and styrene was 1-1.5 times during post-harvest relative to pre-harvest period.

3.5 VOC/acetonitrile emission ratios during pre and post-harvest periods

Emission ratios correlates the emissions of a particular species to that of a reference species, such as CO, CH₃CN, CO₂, C₆H₆. In other words, it is the regression slope of concentration of a particular species versus the reference species (Andreae and Merlet, 2001). Figure 3.5.1 shows the correlations of all the VOCs identified in this work with acetonitrile (chemical marker for biomass burning) in a decreasing order of their correlation in post-harvest period. The black (pre-wheat harvest) and red (post-wheat harvest) dots in the plots are the hourly averaged mixing ratios for each hour of the night between 18:00 to 06:00 L.T. This was done to explore the chemical source signatures of individual VOCs and to have emission

information during the pre-harvest and post-harvest periods (Chandra and Sinha, 2016). Only the nighttime hourly averaged concentrations (18:00 to 06:00 L.T.) were considered to avoid any complications from photochemical formation or loss of compound (mainly due to the reaction of VOCs with hydroxyl radicals in daytime). Different slopes and high absolute concentrations during the post-harvest period in comparison to pre-harvest period is an evidence for altered source signatures in post-harvest period with strong contribution from biomass fires. It appears that the poorly correlated ones are the ones that have strong photochemical source (e.g. isocyanic acid and 2,3-butanedione). This may suggest that lots is left over from daytime formation which is masking the nighttime emission. Table 3.5.1 shows the ratio of average daytime concentration to average nighttime concentration of VOCs during pre-harvest and post-harvest period.



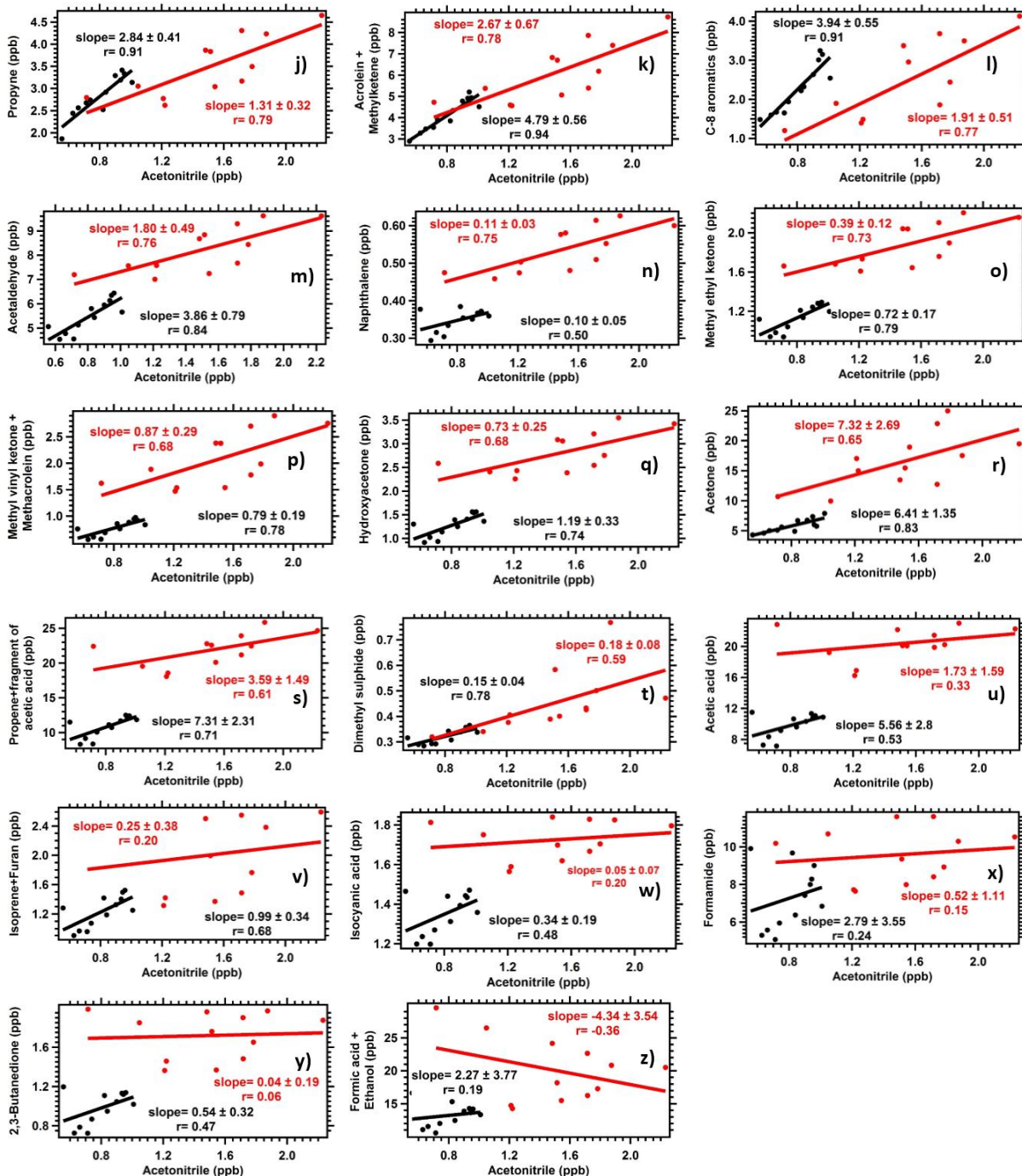


Figure 3.5.1: Correlation plots of all the reported VOCs with acetonitrile in a decreasing order of their correlation. The black (pre-wheat harvest) and red (post-wheat harvest) dots in the plots are the hourly averaged mixing ratios for each hour of the night time between 18:00 to 6:00 L.T. The solid line corresponds to the best-fit straight line through the data points.

Compound	Pre-harvest (avgdaytime/avgnighttime)	Post-harvest (avgdaytime/avgnighttime)
Methanol	0.86	0.93
Acetonitrile	0.77	0.93
Acetaldehyde	1.45	1.60
Acetone	1.04	1.10
DMS	1.08	1.25
Isoprene	1.20	1.24
Methyl vinyl ketone	1.18	1.14
Methyl ethyl ketone	1.28	1.51
Benzene	0.76	0.85
Toluene	0.59	0.63
C-8 aromatics	0.63	0.51
C-9 aromatics	0.65	0.56
Propyne	0.85	0.94
Propene + fragment of acetic acid	1.43	1.75
Isocyanic acid	1.54	1.54
Formamide	1.01	1.09
Formic acid + Ethanol	1.20	1.39
Acrolein + Methylketene	0.86	0.95
Acetamide	0.77	1.06
Acetic acid	1.62	1.78
Nitromethane	1.21	1.32
Hydroxyacetone	1.44	1.53
Assorted Hydrocarbons	1.02	1.12
2,3-Butanedione	1.52	1.70
2-Furaldehyde	1.05	1.13
Styrene	0.67	0.66
Naphthalene	1.17	1.34

Table 3.5.1: Ratio of average daytime concentration to average nighttime concentration of VOCs during pre-harvest and post-harvest period

An estimate of the quanta of VOC emitted from the wheat residue fires can be obtained using the emission ratio of VOCs /acetonitrile along with the acetonitrile/CO emission ratio and the total CO emitted from this activity. About 113 Gg of CO is emitted from wheat crop residue burning during May in Punjab (Badarinath et al., 2006). Using this fact, the amount of

acetonitrile (chemical tracer for biomass burning) emitted from wheat residue fires was calculated by the following equation:

$$\text{Amount of CH}_3\text{CN emitted from wheat residue burning} = \text{CH}_3\text{CN : CO emission ratio} \times \text{Amount of CO emitted from wheat residue burning} \quad (5)$$

Figure 3.5.2 (a) shows the diel box and whisker plot of CO and (b) correlation plot for acetonitrile with CO during pre and post-harvest period. The emission ratio of acetonitrile relative to CO in the post-harvest period was $1.85 \text{ ppb ppm}^{-1}$. The amount of CO emitted from wheat residue burning is already known from the study of Badarinath et al., 2005, therefore, the amount of acetonitrile emitted from wheat residue burning was estimated to be 0.21 Gg. The amount of each VOC emitted from wheat residue burning was calculated using the following equation. The emission ratios of VOCs to CH_3CN were obtained from Figure 3.5.1. This emission estimate was calculated for only those VOCs for which the correlation was better than $r = 0.5$.

$$\text{Amount of VOC emitted from wheat residue burning} = \text{VOC : CH}_3\text{CN emission ratio} \times \text{Amount of CH}_3\text{CN emitted from wheat residue burning} \quad (6)$$

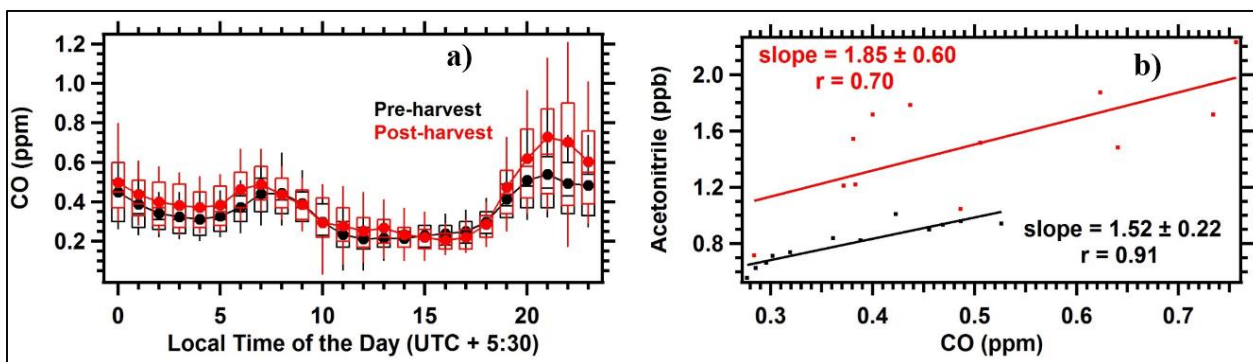


Figure 3.5.2: (a) Diel box and whisker plot of CO; (b) Correlation plot of acetonitrile and carbon monoxide. The black (pre-wheat harvest) and red (post-wheat harvest) dots in the

plots are the hourly averaged mixing ratios for each hour of the night time between 18:00 to 6:00 L.T. The solid line corresponds to the best-fit straight line through the data points.

Figure 3.5.3 summarizes the results in the form of pie chart showing the top ten VOCs that were majorly emitted during the post-wheat harvest period. The major VOC emissions were methanol (5.28 Gg), acetone (1.53 Gg), propene (0.75 Gg) and benzene (0.58 Gg).

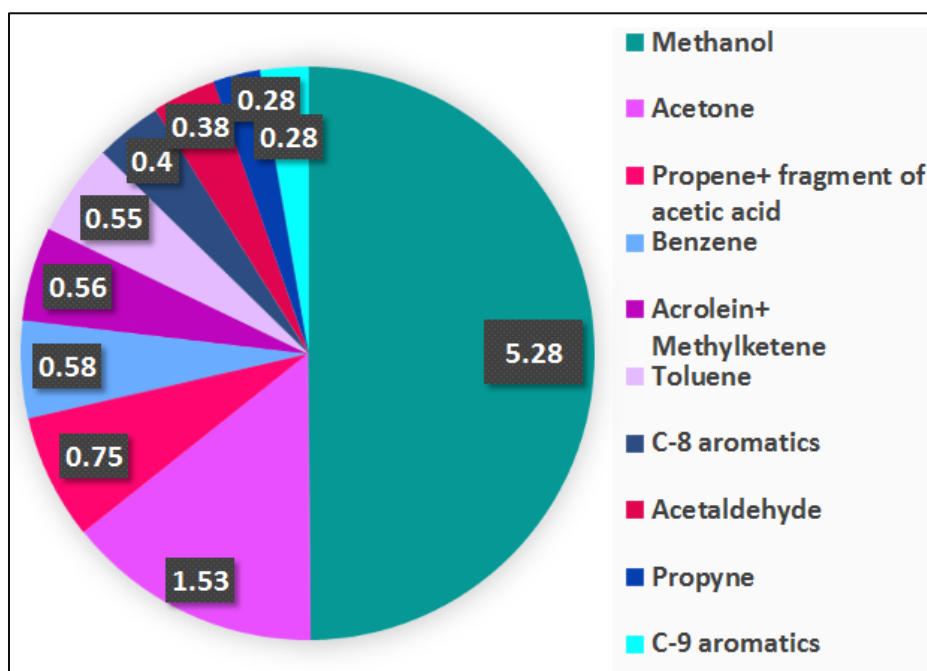
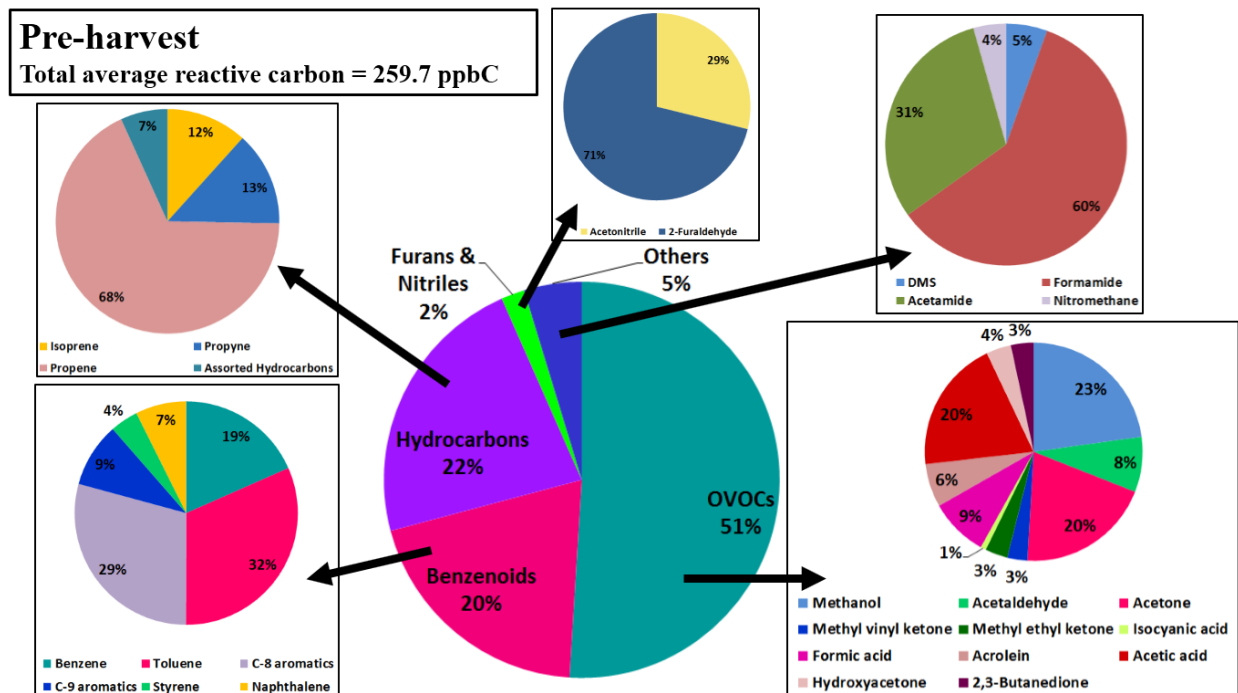


Figure 3.5.3: Major VOCs that were emitted from wheat residue fires.

3.6 Total reactive carbon and ozone production potential of VOCs during pre and post-harvest periods

The total reactive carbon (ppbC) was calculated using the average mixing ratio of each VOC and the number of carbon atoms in its chemical formula. The total average reactive carbon due to all 27 VOCs during pre-harvest and post-harvest period was 259.7 ppbC and 496.6 ppbC, respectively. It means that the total reactive carbon was about 2 times higher in post-harvest period relative to pre-harvest period due to the enhanced average concentrations of VOCs during the wheat residue burning period.



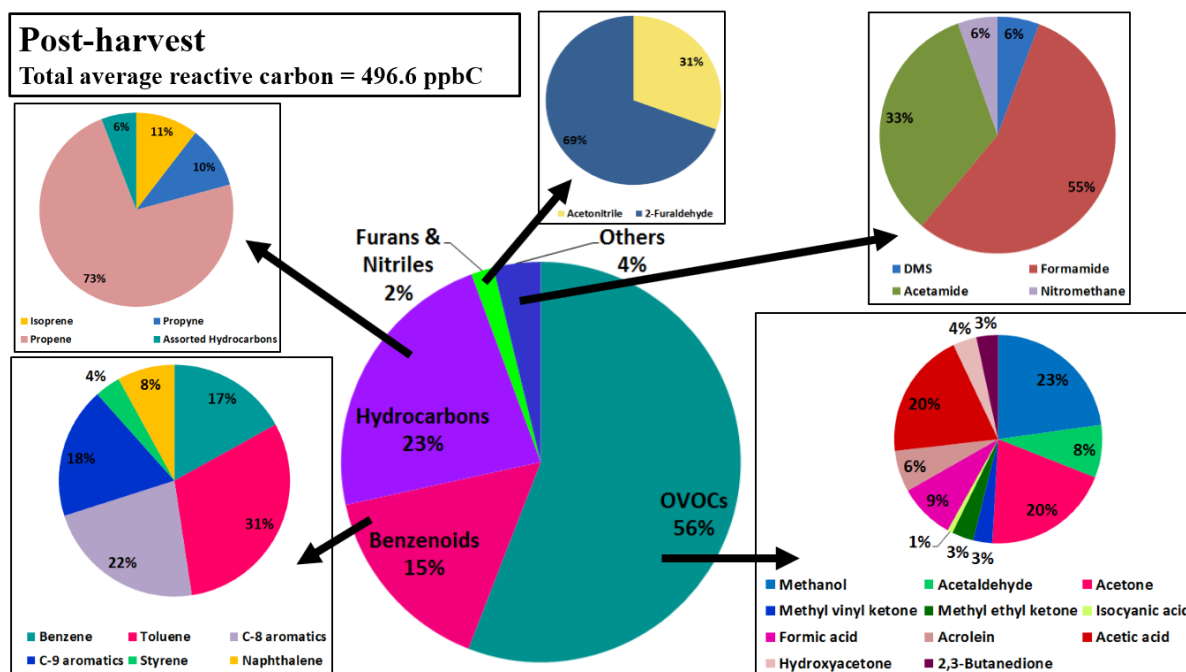


Figure 3.6.1: Pie charts showing the contribution of different class of compounds to total reactive carbon for pre-harvest and post-harvest period.

Pie charts showing the contribution of different class of compounds to total reactive carbon during pre-harvest and post-harvest period are shown in *Figure 3.6.1*.

In general, the largest contributor to total average reactive carbon were oxygenated VOCs (OVOCs; 51 - 56 %), followed by hydrocarbons (22 - 23 %) and benzenoids (15 – 20 %). During the pre-harvest period, the top ten contributing VOCs to the total reactive carbon were propene (15.3 %) > methanol (10.9 %) > acetic acid (10 %) > acetone (7 %) > toluene (6.3 %) > C-8 aromatics (5.8 %) > formic acid (5.6 %) > acetaldehyde (5.2 %) > acrolein (4.5 %) > benzene (3.6 %). These ten compounds together contributed 193 ppbC to the total reactive carbon (259.7 ppbC), which accounts for 74 % of the total reactive carbon in pre-harvest period. During the post-harvest period, the top ten contributing compounds to the total reactive carbon were propene (32 %) > methanol (24.3 %) > acetone (21.3 %) > acetic acid (21.1 %) > formic acid (9.3 %) > toluene (9.2 %) > acetaldehyde (8.8 %) > acrolein (6.9

%) > C-8 aromatics (6.7 %) > C-9 aromatics (5.5 %). These ten compounds together contributed 376.7 ppbC to the total reactive carbon (259.7 ppbC), which accounts for 76 % of the total reactive carbon in post-harvest period.

Ozone is a precursor of hydroxyl radicals which can oxidize most of the atmospheric pollutants. It is formed photochemically in the troposphere through the reactions involving NO_x and trace gases. The ozone production potential of VOCs can be calculated using the following equation (Sinha et al., 2012):

$$\text{O}_3 \text{ production potential} = (\sum k_{(\text{VOC} + \text{OH})} [\text{VOC}]) \times [\text{OH}] \times n \quad (7)$$

where,

$k_{(\text{VOC} + \text{OH})}$ = rate constant for the reaction of VOC with hydroxyl radicals

[VOC] = ambient concentration of VOC

[OH] = average hydroxyl radical concentration

n = number of NO to NO₂ conversions that occur during the photooxidation of VOC

(for VOC emission control n is taken as 2 for all VOCs)

For the ozone formation potential calculations, two time intervals were taken: morning hours (06:00-12:00 LT) and afternoon hours (12:00-18:00 LT) for pre-harvest and post-harvest periods separately. The morning time corresponds to O₃ buildup hours and afternoon time corresponds to the time when O₃ concentrations have reached a plateau. Using the hourly averaged OH radical concentrations, average mixing ratios of VOCs and the temperature corrected rate coefficients of VOCs with OH radicals, the O₃ production potential was calculated. Out of 27 compounds, the rate constants with hydroxyl radicals of 22 VOCs were known. Therefore, the O₃ production potential was calculated only due to 22 VOCs out of 27 and the compounds excluded from the analysis were: isocyanic acid, assorted hydrocarbons, propene, formic acid and acetamide. The rate constants of reaction of VOCs with hydroxyl

radicals were derived from Atkinson and Arey (2003) and NIST chemical kinetics database (<http://kinetics.nist.gov/kinetics>). The results are summarized in Figure 3.6.2. High O₃ formation potential was observed in the period influenced by wheat residue fires as this period is characterized with high concentrations of VOCs and NO_x (Sinha et al., 2014) which are reactive precursors of ozone. The total O₃ production potential during post-harvest period was higher by a factor of 1.7 relative to pre-harvest period for both morning (06:00 to 12:00 LT) and afternoon (12:00 to 18:00 LT) times.

The total O₃ formation potential due to 22 VOCs in the morning time during pre-harvest and post-harvest period was 12.5 ppb h⁻¹ and 21.3 ppb h⁻¹, respectively. The four major contributors to this were isoprene, acetaldehyde, acrolein and 2-furaldehyde, which collectively accounted for 72 % of the total O₃ formation potential.

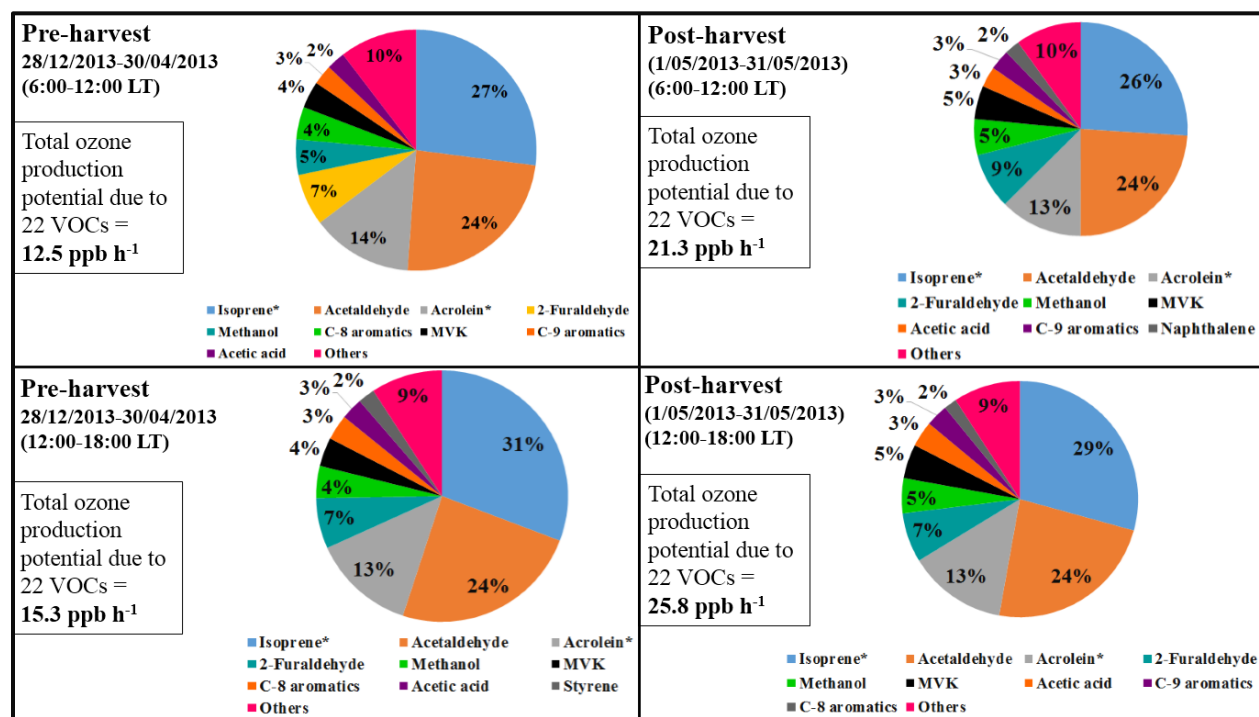


Figure 3.6.2: Contribution of individual VOCs to total O₃ formation potential during pre and post-harvest period for two different time intervals.

The total O₃ formation potential due to 22 VOCs in the afternoon time during pre-harvest and post-harvest period was 15.3 ppb h⁻¹ and 25.8 ppb h⁻¹, respectively. The four major contributors were isoprene, acetaldehyde, acrolein and 2-furaldehyde, which collectively accounted for more than 73 % (73 % for pre-harvest period and 75 % for post-harvest period) of the total O₃ formation potential in the afternoon time.

In afternoon time, an enhancement of 2.8 ppb h⁻¹ of O₃ production potential was observed relative to the morning time in the pre-harvest period, whereas an enhancement of 4.5 ppb h⁻¹ was observed in the post-harvest period. It is because the [OH] is usually high (~10⁶ molecules cm⁻³) in the afternoon time and hence the ozone production potential is driven by the OH radical concentrations. Thus, the in-situ ozone formation is strongly influenced by wheat residue burning activity. These results also help explain the 19 ppb enhancement in surface O₃ concentrations during post-wheat harvest period as reported by Kumar et al. (2016). The increased organic reactivity in air contributes as a reactive fuel for surface O₃ production.

3.7 SOA formation potential of VOCs

The oxidation of VOCs and semi volatile organic compounds (SVOCs) in the gas phase, forms less volatile products which can then partition to particle-phase and hence form secondary organic aerosols (SOA). It can significantly contribute to particulate burden. The SOA produced from oxidation of VOCs (SOA_{cal}) can be calculated using the following equation:

$$\text{SOA}_{\text{cal}} = \sum [\text{VOC}] \times [\text{Y}_i] \quad (8)$$

where,

[VOC] = ambient concentration of VOC

Y_i = SOA yields of various VOCs reported in literature

Table 3.7.1 shows the SOA yields of aromatic VOCs. SOA formation potential of isoprene, benzene, toluene, xylenes, trimethylbenzenes, naphthalene and styrene is shown in *Figure 3.7.1*.

VOCs	SOA Yields (%)	References
Isoprene	2 %	Lee et al. (2006)
Benzene	26.3 %	Ng et al. (2007)
Toluene	12 %	Ng et al. (2007)
Xylenes	7.2 %	Ng et al. (2007)
Trimethylbenzenes	7.2 %	Yuan et al. (2013)
Styrene	7.2 %	Yuan et al. (2013)
Naphthalene	30.8 %	Chan et al. (2009)

Table 3.7.1: SOA yields of VOCs

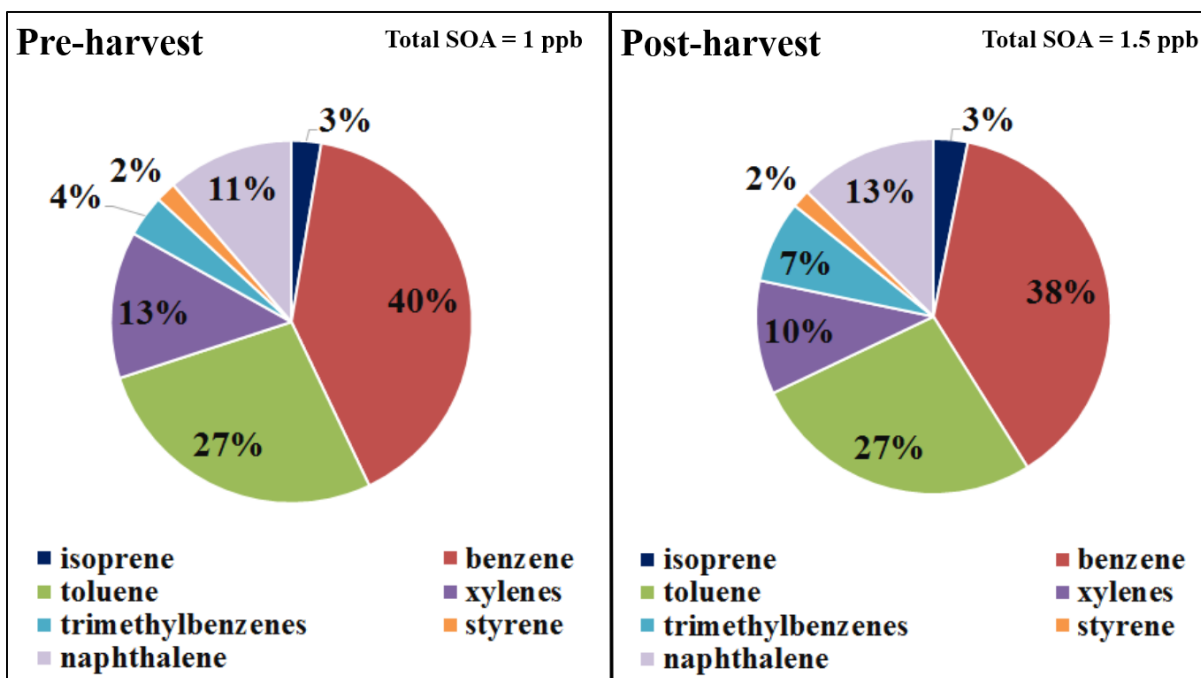


Figure 3.7.1: SOA formation potential of isoprene, benzene, toluene, xylenes, trimethylbenzenes, naphthalene and styrene

The SOA production potential was calculated for 7 VOCs: isoprene, toluene, benzene, toluene, xylenes, trimethylbenzenes, naphthalene and styrene. The SOA formation potential of 7 VOCs during post-harvest period was 1.5 times higher relative to pre-harvest period. The order of SOA formation potential for these VOCs in pre-harvest period was benzene (0.42 ppb) > toluene (0.28 ppb) > xylenes (0.14 ppb) > naphthalene (0.12 ppb) > trimethylbenzenes (0.04 ppb) > isoprene (0.03 ppb) > styrene (0.02 ppb). The order of SOA formation potential for these VOCs in post-harvest period was benzene (0.58 ppb) > toluene (0.41 ppb) > naphthalene (0.19 ppb) > xylenes (0.16 ppb) > trimethylbenzenes (0.11 ppb) > isoprene (0.05 ppb) > styrene (0.02 ppb).

3.8 Evaluation of a method for estimating anthropogenic contribution to VOC concentrations

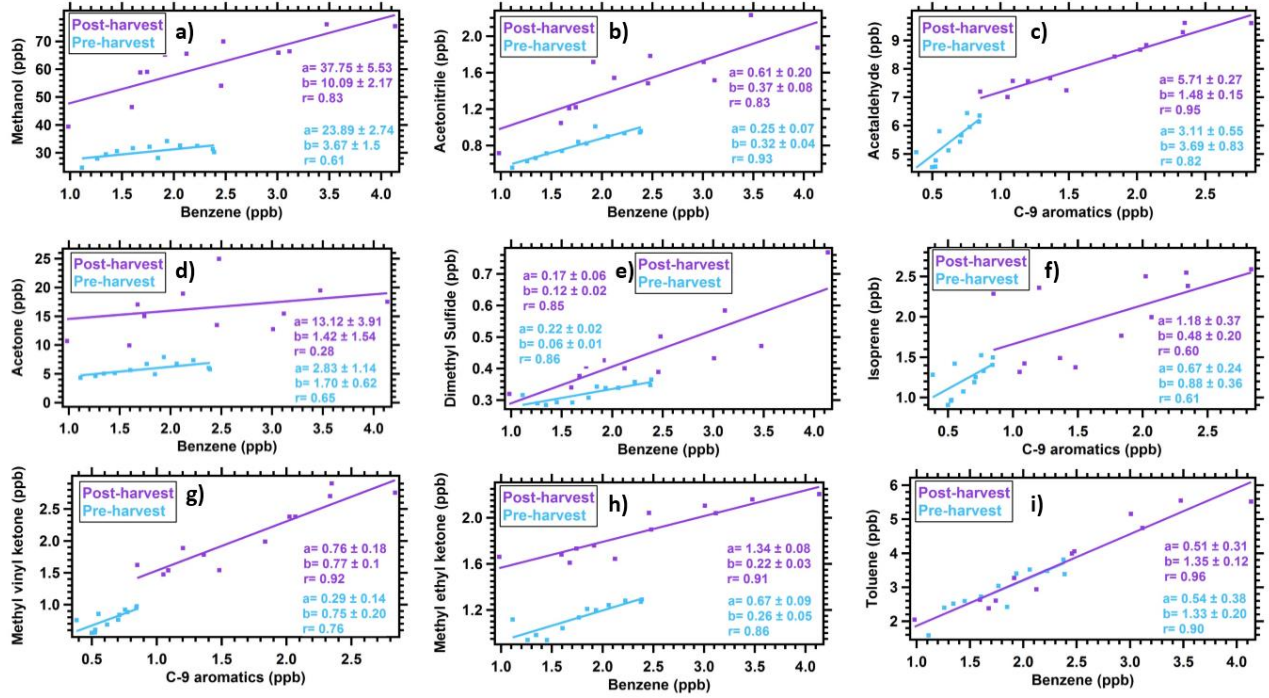
To estimate the anthropogenic contribution to the measured VOC concentrations, Riemann et al. proposed a method (Reimann et al., 2000). For this analysis, the mixing ratios of C-9 aromatics and benzene were used as the anthropogenic tracers since non-anthropogenic sources are negligible for these two compounds (Sahu et al., 2016). Firstly, the molar ratio of each VOC to benzene or C-9 aromatics ($\Delta\text{VOC}/\Delta\text{benzene}$ or C-9 aromatics) was determined explicitly using the nighttime data for both pre-harvest and post-harvest period as shown in *Figure 3.8.1*. The nighttime conditions were chosen since no biogenic emissions or photochemical formation takes place in the night and any emissions would be attributed only to the anthropogenic emissions. The nighttime data set represents insignificant change in VOC composition due to lack of OH radicals and hence lack of oxidation. Therefore, this ratio can be understood as the ratio between anthropogenic VOC and benzene/C-9 aromatics. We assume that the molar ratio between anthropogenic VOC and benzene/C-9 aromatics does not fluctuate with time. Another assumption of this method is that the VOC whose anthropogenic fraction is to be estimated and benzene/C-9 aromatics has the same rate for the reaction with OH radicals. The VOCs whose reaction rate with OH is in the range of 10^{-11} - 10^{-10} $\text{cm}^3 \text{ molecule}^{-1} \text{ s}^{-1}$, the molar ratio for them was calculated with C-9 aromatics ($k_{\text{C-9 aromatics}+\text{OH}} = 3.25 \times 10^{-11} \text{ cm}^3 \text{ molecule}^{-1} \text{ s}^{-1}$; Atkinson et al., 2003) and those VOCs whose reaction rate with OH is in the range of 10^{-13} - 10^{-12} $\text{cm}^3 \text{ molecule}^{-1} \text{ s}^{-1}$, the molar ratio for them was calculated with benzene ($k_{\text{benzene}+\text{OH}} = 1.19 \times 10^{-12} \text{ cm}^3 \text{ molecule}^{-1} \text{ s}^{-1}$; Atkinson et al., 2003).

The anthropogenic contribution and the percentage anthropogenic contribution was calculated using the following equation:

$$\text{Anthropogenic Contribution of VOC} = [\Delta\text{VOC}/\Delta\text{Benzene or C-9 aromatics}]_{(\text{night})} \times \text{Benzene or C-9 aromatics} \quad (9)$$

Percentage anthropogenic contribution = (Anthropogenic contribution/Measured total VOC) *100

(10)



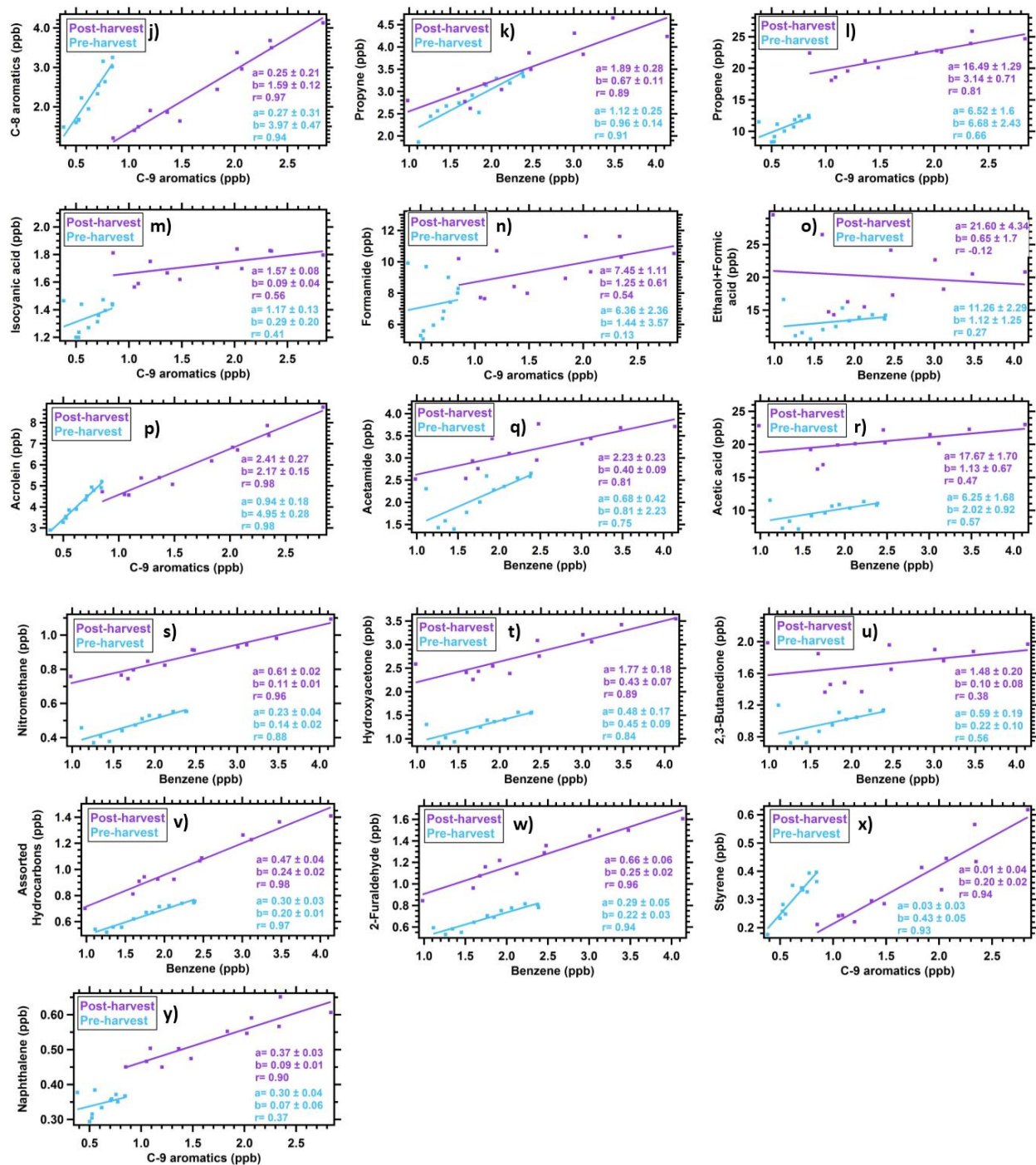
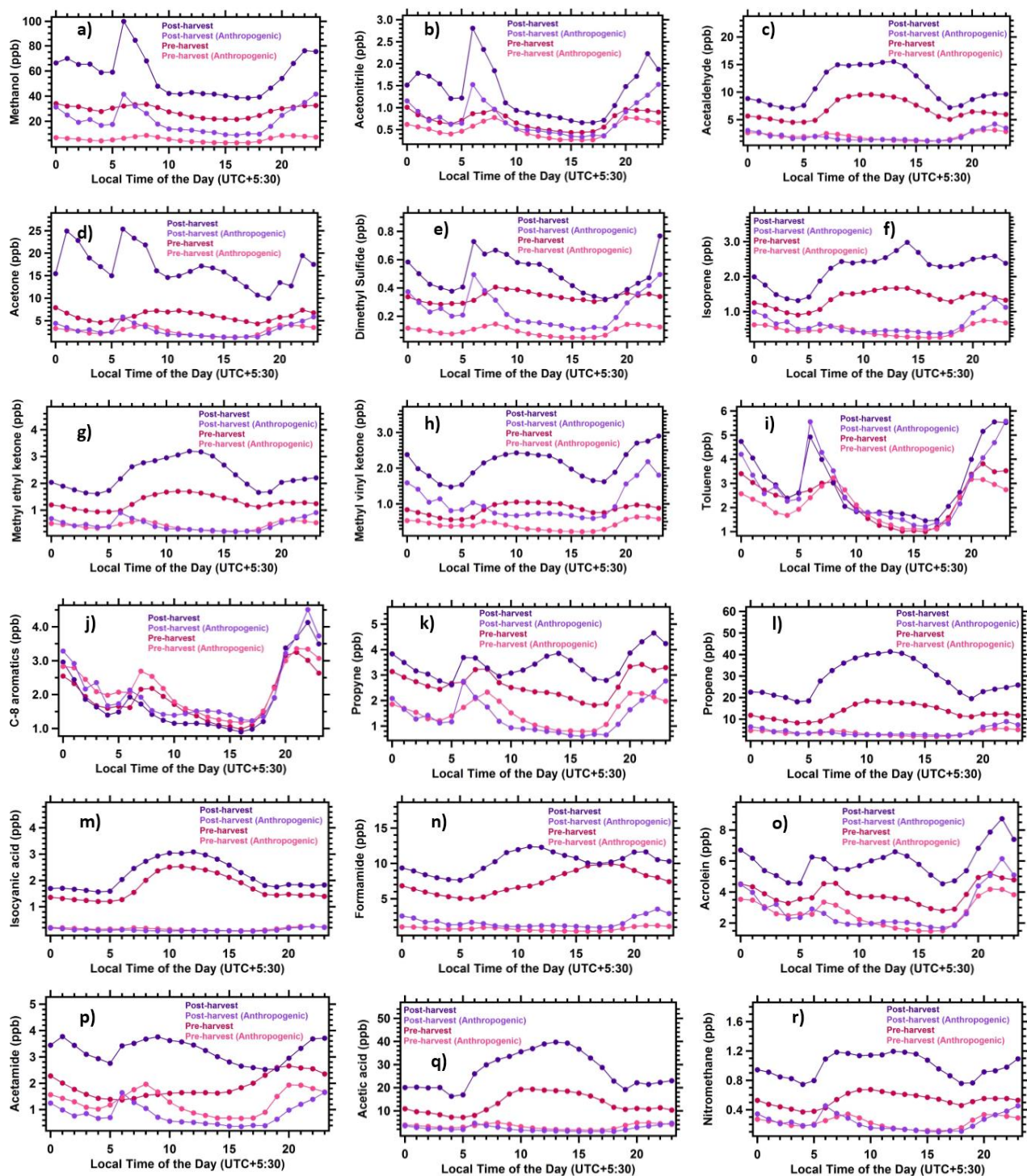


Figure 3.8.1: Scatter plots of all the VOCs versus benzene/C-9 aromatics. The light-blue (pre-wheat harvest) and purple (post-wheat harvest) markers in the plots are the hourly averaged mixing ratios for each hour of the night between 18:00 to 6:00 L.T. The solid line

corresponds to the best-fit straight line through the data points and the regression equations and correlation coefficients are also indicated.

Diurnal profile of anthropogenic contribution and observed total concentration of VOC during pre-harvest and post-harvest period is shown in *Figure 3.8.2*. *Figure 3.8.3* shows the anthropogenic fraction of each VOC during pre-harvest and post-harvest period. One would expect that the anthropogenic fraction of all the VOCs would be higher in the post-harvest period as it is marked with enhanced anthropogenic biomass burning activities in comparison to pre-harvest period. But, the results were counter-intuitive as the percentage anthropogenic contribution to VOCs was lower in post-harvest period except for methanol, dimethyl sulfide and formamide. For VOCs such as methanol, acetonitrile, dimethyl sulfide, isoprene, methyl ethyl ketone, toluene and assorted hydrocarbons, the absolute mixing ratio of anthropogenic contribution to VOCs was higher in post-harvest period relative to pre-harvest period. The absolute mixing ratio of anthropogenic contribution of acetonitrile (a chemical tracer for biomass burning) in post-harvest season were comparable to its total concentrations in pre-harvest season. The absolute mixing ratio of anthropogenic contribution to VOCs in pre-harvest period for most of the oxygenates ($C_xH_yO_z$), for example, acetaldehyde, acetone, MEK, isocyanic acid, acetamide, acetic acid, nitromethane, hydroxyacetone and 2,3-butanedione, were comparable to their absolute mixing ratio of anthropogenic contribution in post-harvest period. It suggests that the anthropogenic contribution to OVOCs has not changed much in pre-harvest and post-harvest period.

It is noteworthy that the ERs of $\Delta\text{VOC}/\Delta\text{Benzene}$ or C-9 aromatics are associated with large uncertainties as the tracers, i.e., benzene and C-9 aromatics, do not represent the primary emission from a single type of source. Both the tracers have multiple sources in the urban environment, for example, biomass burning, biofuel burning and vehicular exhaust emissions. Also, the diurnal pattern of OVOCs, such as acetaldehyde, acetone, isocyanic acid, MVK, MEK and acetic acid is very different from those of the anthropogenic tracers. These could be the reasons why this method is not an efficient method in estimating anthropogenic contribution to VOCs.



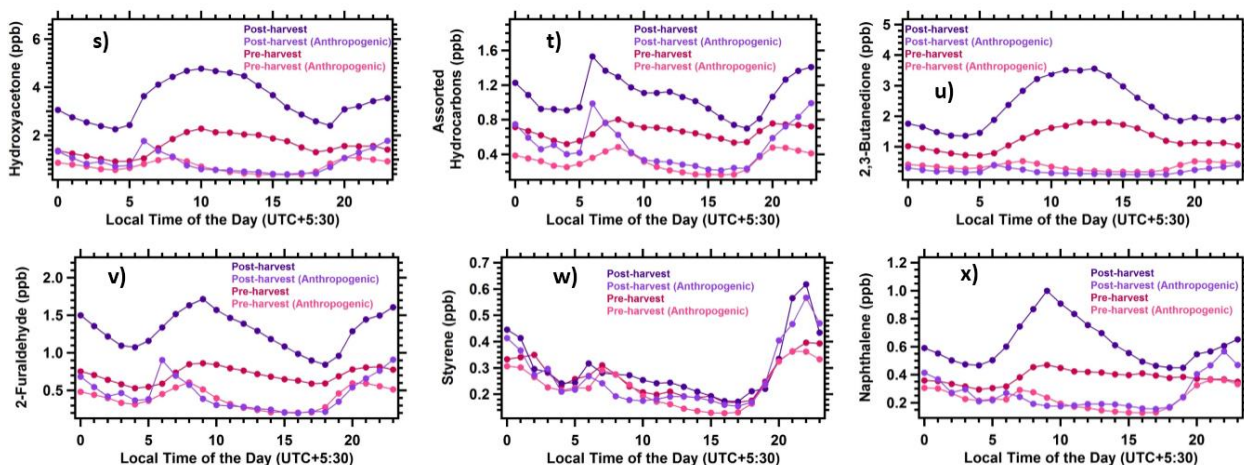
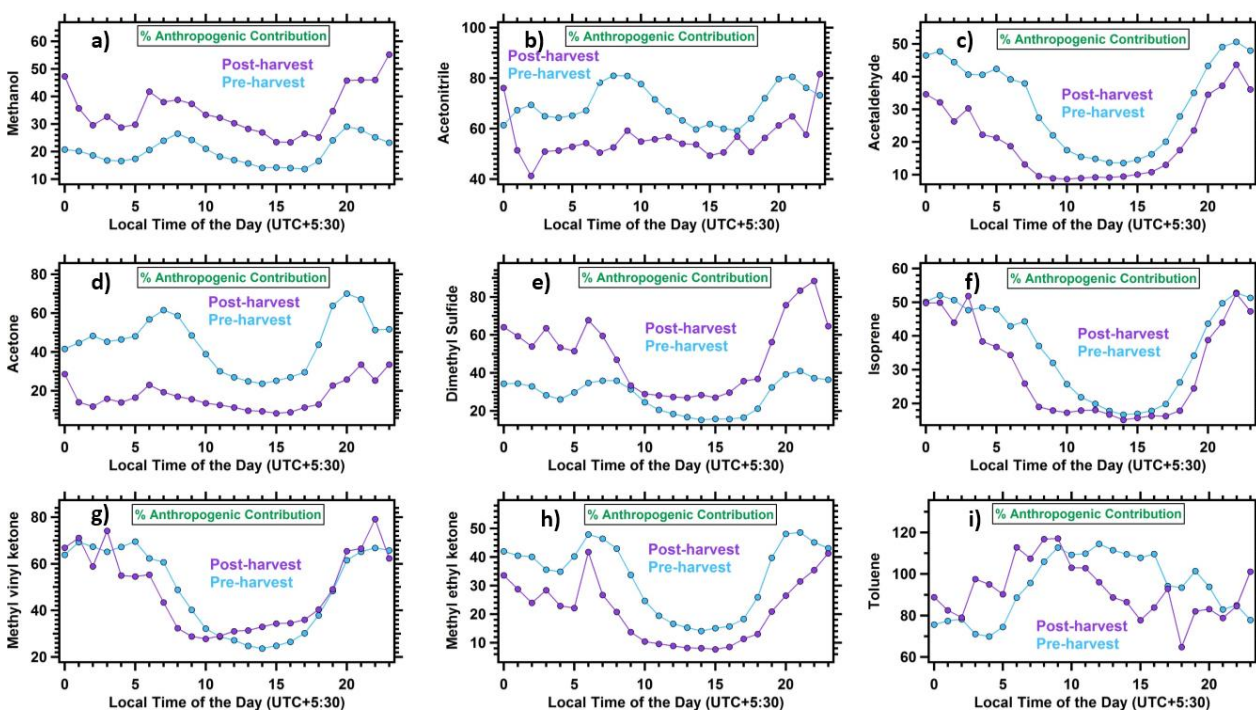


Figure 3.8.2: Diurnal profile of anthropogenic contribution and observed total concentration of VOCs during pre and post-harvest period



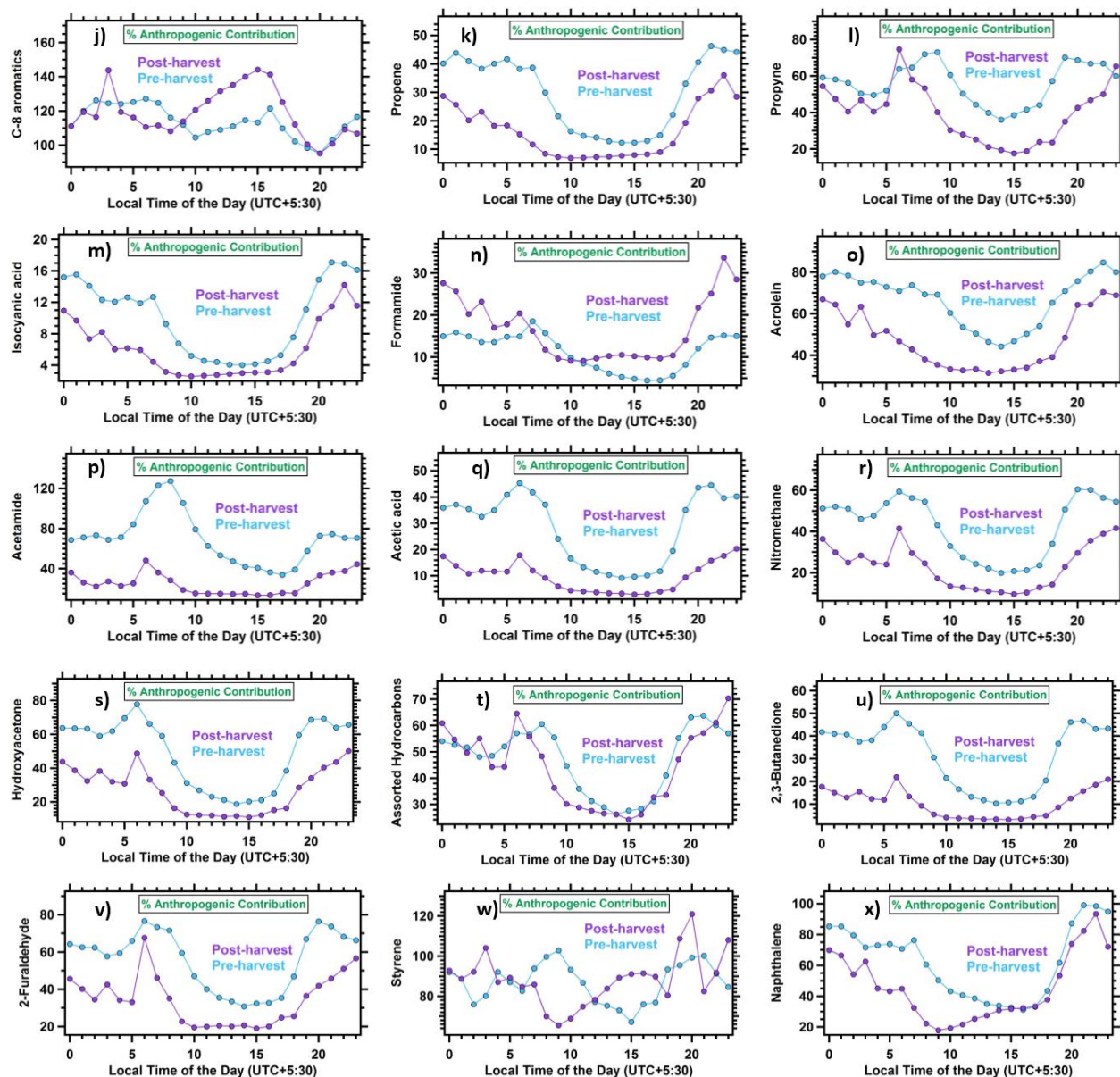


Figure 3.8.3: Anthropogenic fraction of all the VOCs during the pre-harvest and post-harvest period. The light-blue (pre-harvest) and purple (post-harvest) markers are the hourly averaged mixing ratios

Chapter 4

4 Summary and conclusion

The deployment of novel PTR-MS technique allowed us the detection of VOCs from wheat residue fires at a temporal resolution of 1 minute for the first time in N.W.IGP. A total of 27 different organic compounds were identified which were attributed to post-harvest wheat residue fires (at a confidence interval of $> 99.99\%$). 14 out of 27 compounds were reported for the first time over N.W. IGP from wheat residue burning and those newly reported compounds are propyne, propene, formamide, formic acid, acrolein, methylketene, acetamide, acetic acid, nitromethane, hydroxyacetone, 2,3-butanedione, 2-furaldehyde, styrene and naphthalene. A new compound, i.e., 2,3-butanedione ($m/z = 87$) was identified for the first time in ambient Indian air and C-9 aromatics were identified as one of the precursors but there must certainly be more precursors, as the observed concentrations cannot be explained only on the basis of the C-9 precursor compounds. The average mixing ratios (average $\pm 1\sigma$ ambient variability) of acetonitrile (1.35 ± 1.30 ppb) and 2,3-butanedione (2.35 ± 1.08 ppb) in post-harvest period were higher by a factor of 1.8 relative to pre-harvest period. Different VOC/acetonitrile emission ratios and high absolute concentrations during post-harvest period in comparison to pre-harvest period suggests altered source signatures in post-harvest period with strong contribution from biomass fires. Methanol (5.28 Gg), acetone (1.53 Gg), propene (0.75 Gg) and benzene (0.58 Gg) were the four predominantly emitted species from wheat residue fires. The total average reactive carbon due to all 27 VOCs during pre-harvest and post-harvest period was 259.7 ppbC and 496.6 ppbC, respectively. It means that the total average reactive carbon was 2 times higher in post-harvest period relative to pre-harvest period. The total O₃ production potential due to 22 VOCs during post-harvest period was higher by a factor of 1.7 relative to pre-harvest period for both morning

(06:00 to 12:00 LT) and afternoon (12:00 to 18:00 LT) times. The four major contributors to total O₃ formation potential were isoprene, acetaldehyde, acrolein and 2-furaldehyde, which collectively accounted for more than 72 % of the total O₃ formation potential. The SOA formation potential of VOCs pre-harvest period was in the following order: benzene > toluene > xylenes > naphthalene > trimethylbenzenes > isoprene > styrene, whereas in post-harvest period the order was: benzene > toluene > naphthalene > xylenes > trimethylbenzenes > isoprene > styrene. We also examined the method proposed by Reimann et al. (2000) to estimate the anthropogenic fraction of VOCs using the mixing ratio of C-9 aromatics and benzene as a reference for anthropogenic emissions. This method is not an efficient and reliable method in constraining the anthropogenic fraction of VOCs.

As the ambient chemical mixture has high concentrations of both reactive aromatic compounds and oxidants, the potential for chemical transformations and reactions of aromatic compounds to form aerosol and fuel ozone production locally on short time scales (few hours) appears to be particularly high and is important to consider for mitigation strategies. To better understand the overall picture, we must also obtain the EF measurements, combustion efficiency and its characteristics. This should be made a priority area for future research. There is an urgent need to design appropriate mitigation strategies to control the emissions from open wheat residue burning. Rather than burning of wheat residue, the retention of wheat straw in soil has been considered as a safer practice since it has a potential to increase microbial biomass and thus improving the soil fertility (Kushwaha and Singh, 2005).

5 Bibliography

- AKAGI, S. K., YOKELSON, R. J., WIEDINMYER, C., ALVARADO, M. J., REID, J. S., KARL, T., CROUNSE, J. D. & WENNERBERG, P. O. 2011. Emission factors for open and domestic biomass burning for use in atmospheric models. *Atmos. Chem. Phys.*, 11, 4039-4072.
- ANDREAE, M. O. & MERLET, P. 2001. Emission of trace gases and aerosols from biomass burning. *Global Biogeochemical Cycles*, 15, 955-966.
- ATKINSON, R. & AREY, J. 2003. Atmospheric degradation of volatile organic compounds. *Chemical reviews*, 103, 4605-4638.
- ATKINSON, R., CARTER, W. P. & WINER, A. M. 1983. Effects of pressure on product yields in the nitrogen oxide (NO_x) photooxidations of selected aromatic hydrocarbons. *The Journal of Physical Chemistry*, 87, 1605-1610.
- BADARINATH, K., CHAND, T. & PRASAD, V. 2006. the Indo-Gangetic Plains—A study using IRS-P6 AWiFS satellite data. *Current Science*, 91, 1085.
- BANDOW, H. & WASHIDA, N. 1985a. Ring-cleavage Reactions of Aromatic Hydrocarbons Studied by FT-IR Spectroscopy. II. Photooxidation of o-, m-, and p-Xylenes in the NO_x-Air System. *Bulletin of the Chemical Society of Japan*, 58, 2541-2548.
- BANDOW, H. & WASHIDA, N. 1985b. Ring-cleavage Reactions of Aromatic Hydrocarbons Studied by FT-IR Spectroscopy. III. Photooxidation of 1, 2, 3-, 1, 2, 4-, and 1, 3, 5-Trimethylbenzenes in the NO_x-Air System. *Bulletin of the Chemical Society of Japan*, 58, 2549-2555.
- BRILLI, F., GIOLI, B., CICCIOLO, P., ZONA, D., LORETO, F., JANSSENS, I. A. & CEULEMANS, R. 2014. Proton Transfer Reaction Time-of-Flight Mass Spectrometric (PTR-TOF-MS) determination of volatile organic compounds (VOCs) emitted from a biomass fire developed under stable nocturnal conditions. *Atmospheric Environment*, 97, 54-67.
- BRUNO, P., CASELLI, M., DE GENNARO, G., SCOLLETTA, L., TRIZIO, L. & TUTINO, M. 2008. Assessment of the impact produced by the traffic source on VOC level in the urban area of Canosa di Puglia (Italy). *Water, air, and soil pollution*, 193, 37-50.
- BUCZYNSKA, A. J., KRATA, A., STRANGER, M., GODOI, A. F. L., KONTOZOVA-DEUTSCH, V., BENCS, L., NAVEAU, I., ROEKENS, E. & VAN GRIEKEN, R. 2009. Atmospheric BTEX-concentrations in an area with intensive street traffic. *Atmospheric Environment*, 43, 311-318.
- CHAN, A. W. H., KAUTZMAN, K. E., CHHABRA, P. S., SURRATT, J. D., CHAN, M. N., CROUNSE, J. D., KÜRTEN, A., WENNERBERG, P. O., FLAGAN, R. C. & SEINFELD, J. H. 2009. Secondary organic aerosol formation from photooxidation of naphthalene and alkylnaphthalenes: implications for oxidation of intermediate volatility organic compounds (IVOCs). *Atmospheric Chemistry and Physics*, 9, 3049-3060.
- CHANDRA, B. P. & SINHA, V. 2016. Contribution of post-harvest agricultural paddy residue fires in the N.W. Indo-Gangetic Plain to ambient carcinogenic benzenoids, toxic isocyanic acid and carbon monoxide. *Environment International*, 88, 187-197.
- DAGAUT, P., WALLINGTON, T. J., LIU, R. & KURYLO, M. J. 1988. A kinetic investigation of the gas-phase reactions of hydroxyl radicals with cyclic ketones and diones: mechanistic insights. *The Journal of Physical Chemistry*, 92, 4375-4377.

- DARNALL, K. R., ATKINSON, R. & PITTS, J. N. 1979. Observation of biacetyl from the reaction of OH radicals with o-xylene. Evidence for ring cleavage. *Journal of Physical Chemistry*, 83, 1943-1946.
- DE GOUW, J., WARNEKE, C., KARL, T., EERDEKENS, G., VAN DER VEEN, C. & FALL, R. 2003. Sensitivity and specificity of atmospheric trace gas detection by proton-transfer-reaction mass spectrometry. *International Journal of Mass Spectrometry*, 223, 365-382.
- GOLDSTEIN, A. H. & GALBALLY, I. E. 2007. Known and unexplored organic constituents in the earth's atmosphere. *Environmental Science & Technology*, 41, 1514-1521.
- GROS, V., GAIMOZ, C., HERRMANN, F., CUSTER, T., WILLIAMS, J., BONSAING, B., SAUVAGE, S., LOCOGE, N., D'ARGOUGES, O. & SARDA-ESTÈVE, R. 2011. Volatile organic compounds sources in Paris in spring 2007. Part I: qualitative analysis. *Environmental Chemistry*, 8, 74-90.
- KARL, T., CHRISTIAN, T. J., YOKELSON, R. J., ARTAXO, P., HAO, W. M. & GUENTHER, A. 2007. The Tropical Forest and Fire Emissions Experiment: method evaluation of volatile organic compound emissions measured by PTR-MS, FTIR, and GC from tropical biomass burning. *Atmospheric Chemistry and Physics*, 7, 5883-5897.
- KARL, T., JOBSON, T., KUSTER, W. C., WILLIAMS, E., STUTZ, J., SHETTER, R., HALL, S. R., GOLDAN, P., FEHSENFELD, F. & LINDINGER, W. 2003. Use of proton-transfer-reaction mass spectrometry to characterize volatile organic compound sources at the La Porte super site during the Texas Air Quality Study 2000. *Journal of Geophysical Research: Atmospheres (1984–2012)*, 108.
- KATO, S., MIYAKAWA, Y., KANEKO, T. & KAJII, Y. 2004. Urban air measurements using PTR-MS in Tokyo area and comparison with GC-FID measurements. *International Journal of Mass Spectrometry*, 235, 103-110.
- KHODER, M. 2007. Ambient levels of volatile organic compounds in the atmosphere of Greater Cairo. *Atmospheric Environment*, 41, 554-566.
- KOUKOL, J., DUGGER, W. & PALMER, R. 1967. Inhibitory effect of peroxyacetyl nitrate on cyclic photophosphorylation by chloroplasts from black valentine bean leaves. *Plant physiology*, 42, 1419-1422.
- KUMAR, V., SARKAR, C. & SINHA, V. 2016. Influence of post-harvest crop residue fires on surface ozone mixing ratios in the NW IGP analyzed using 2 years of continuous in situ trace gas measurements. *Journal of Geophysical Research: Atmospheres*, 121, 3619-3633.
- KUMAR, V. & SINHA, V. 2014. VOC–OHM: A new technique for rapid measurements of ambient total OH reactivity and volatile organic compounds using a single proton transfer reaction mass spectrometer. *International Journal of Mass Spectrometry*, 374, 55-63.
- KUSHWAHA, C. & SINGH, K. 2005. Crop productivity and soil fertility in a tropical dryland agro-ecosystem: impact of residue and tillage management. *Experimental Agriculture*, 41, 39-50.
- LAMB, B., VELASCO, E., ALLWINE, E., WESTBERG, H., HERNDON, S., KNIGHTON, B. & GRIMSRUD, E. Ambient VOC measurements in Mexico City during the MCMA 2002 and 2003 field campaigns. Sixth Conference on Atmospheric Chemistry: Air Quality in Megacities, American Meteorol. Soc., Seattle, WA, 2004.

- LEE, A., GOLDSTEIN, A. H., KROLL, J. H., NG, N. L., VARUTBANGKUL, V., FLAGAN, R. C. & SEINFELD, J. H. 2006. Gas-phase products and secondary aerosol yields from the photooxidation of 16 different terpenes. *Journal of Geophysical Research: Atmospheres*, 111.
- LINDINGER, W., HANSEL, A. & JORDAN, A. 1998. On-line monitoring of volatile organic compounds at pptv levels by means of proton-transfer-reaction mass spectrometry (PTR-MS) medical applications, food control and environmental research. *International Journal of Mass Spectrometry and Ion Processes*, 173, 191-241.
- LIU, J., MU, Y., ZHANG, Y., ZHANG, Z., WANG, X., LIU, Y. & SUN, Z. 2009. Atmospheric levels of BTEX compounds during the 2008 Olympic Games in the urban area of Beijing. *Science of The Total Environment*, 408, 109-116.
- MALEKNIA, S. D., BELL, T. L. & ADAMS, M. A. 2007. PTR-MS analysis of reference and plant-emitted volatile organic compounds. *International Journal of Mass Spectrometry*, 262, 203-210.
- MCKERNAN, L. T., NIEMEIER, R. T., KREISS, K., PARK, R., DANKOVIC, D. A., DUNN, K. H., PARKER, J. A., FEDAN, K. B., STREICHER, R. P. & FEDAN, J. S. 2016. Occupational.
- MILLER, L., XU, X., GRGICAK-MANNION, A., BROOK, J. & WHEELER, A. 2012. Multi-season, multi-year concentrations and correlations amongst the BTEX group of VOCs in an urbanized industrial city. *Atmospheric Environment*, 61, 305-315.
- MÜLLER, M., ANDERSON, B. E., BEYERSDORF, A. J., CRAWFORD, J. H., DISKIN, G. S., EICHLER, P., FRIED, A., KEUTSCH, F. N., MIKOVINY, T. & THORNHILL, K. L. 2016. In situ measurements and modeling of reactive trace gases in a small biomass burning plume. *Atmospheric Chemistry and Physics*, 16, 3813-3824.
- NG, N., KROLL, J., CHAN, A., CHHABRA, P., FLAGAN, R. & SEINFELD, J. 2007. Secondary organic aerosol formation from m-xylene, toluene, and benzene. *Atmospheric Chemistry and Physics*, 7, 3909-3922.
- NOJIMA, K., FUKAYA, K., FUKUI, S. & KANNO, S. 1974. The formation of glyoxals by the photochemical reaction of aromatic hydrocarbons in the presence of nitrogen monoxide. *Chemosphere*, 3, 247-252.
- PAWAR, H., GARG, S., KUMAR, V., SACHAN, H., ARYA, R., SARKAR, C., CHANDRA, B. & SINHA, B. 2015. Quantifying the contribution of long-range transport to particulate matter (PM) mass loadings at a suburban site in the north-western Indo-Gangetic Plain (NW-IGP). *Atmospheric Chemistry and Physics*, 15, 9501-9520.
- PLUM, C. N., SANHUEZA, E., ATKINSON, R., CARTER, W. P. & PITTS, J. N. 1983. Hydroxyl radical rate constants and photolysis rates of. α -dicarbonyls. *Environmental science & technology*, 17, 479-484.
- REIMANN, S., CALANCA, P. & HOFER, P. 2000. The anthropogenic contribution to isoprene concentrations in a rural atmosphere. *Atmospheric Environment*, 34, 109-115.
- RODIGAST, M., MUTZEL, A., SCHINDELKA, J. & HERRMANN, H. 2016. A new source of methylglyoxal in the aqueous phase. *Atmospheric Chemistry and Physics*, 16, 2689-2702.
- SAHAI, S., SHARMA, C., SINGH, D. P., DIXIT, C. K., SINGH, N., SHARMA, P., SINGH, K., BHATT, S., GHUDE, S., GUPTA, V., GUPTA, R. K., TIWARI, M. K., GARG, S. C., MITRA, A. P. & GUPTA, P. K. 2007. A study for development of emission factors for trace gases and carbonaceous particulate species from in situ burning of wheat straw in agricultural fields in india. *Atmospheric Environment*, 41, 9173-9186.

- SAHU, L., YADAV, R. & PAL, D. 2016. Source identification of VOCs at an urban site of western India: Effect of marathon events and anthropogenic emissions. *Journal of Geophysical Research: Atmospheres*.
- SARKAR, C., SINHA, V., KUMAR, V., RUPAKHETI, M., PANDAY, A., MAHATA, K. S., RUPAKHETI, D., KATHAYAT, B. & LAWRENCE, M. G. 2016. Overview of VOC emissions and chemistry from PTR-TOF-MS measurements during the SusKat-ABC campaign: high acetaldehyde, isoprene and isocyanic acid in wintertime air of the Kathmandu Valley. *Atmos. Chem. Phys*, 16, 3979-4003.
- SHEPSON, P., EDNEY, E. & CORSE, E. 1984. Ring fragmentation reactions on the photooxidations of toluene and o-xylene. *Journal of physical chemistry*, 88, 4122-4126.
- SINHA, V., KUMAR, V. & SARKAR, C. 2014. Chemical composition of pre-monsoon air in the Indo-Gangetic Plain measured using a new air quality facility and PTR-MS: high surface ozone and strong influence of biomass burning. *Atmospheric Chemistry and Physics*, 14, 5921-5941.
- SINHA, V., WILLIAMS, J., DIESCH, J., DREWNICK, F., MARTINEZ, M., HARDER, H., REGELIN, E., KUBISTIN, D., BOZEM, H. & HOSAYNALI-BEYGI, Z. 2012. Constraints on instantaneous ozone production rates and regimes during DOMINO derived using in-situ OH reactivity measurements. *Atmospheric Chemistry and Physics*, 12, 7269-7283.
- STOCKWELL, C., VERES, P., WILLIAMS, J. & YOKELSON, R. 2015. Characterization of biomass burning emissions from cooking fires, peat, crop residue, and other fuels with high-resolution proton-transfer-reaction time-of-flight mass spectrometry. *Atmospheric Chemistry and Physics*, 15, 845-865.
- TAKAGI, H., WASHIDA, N., AKIMOTO, H., NAGASAWA, K., USUI, Y. & OKUDA, M. 1980. Photooxidation of o-xylene in the nitric oxide-water-air system. *The Journal of Physical Chemistry*, 84, 478-483.
- TUAZON, E. C., MAC LEOD, H., ATKINSON, R. & CARTER, W. P. 1986. Alpha-dicarbonyl yields from the NO_x-air photooxidations of a series of aromatic hydrocarbons in air. California Univ., Riverside (USA). Statewide Air Pollution Research Center.
- VENKATARAMAN, C., HABIB, G., KADAMBA, D., SHRIVASTAVA, M., LEON, J. F., CROUZILLE, B., BOUCHER, O. & STREETS, D. G. 2006. Emissions from open biomass burning in India: Integrating the inventory approach with high-resolution Moderate Resolution Imaging Spectroradiometer (MODIS) active-fire and land cover data. *Global Biogeochemical Cycles*, 20, n/a-n/a.
- YOKELSON, R. J., CHRISTIAN, T. J., KARL, T. G. & GUENTHER, A. 2008. The tropical forest and fire emissions experiment: laboratory fire measurements and synthesis of campaign data. *Atmos. Chem. Phys.*, 8, 3509-3527.
- YUAN, B., HU, W., SHAO, M., WANG, M., CHEN, W., LU, S., ZENG, L. & HU, M. 2013. VOC emissions, evolutions and contributions to SOA formation at a receptor site in eastern China. *Atmospheric Chemistry and Physics*, 13, 8815-8832.